Computing uncertainties in ionosphere-airglow models: II. The Martian airglow

Guillaume Gronoff,[1] Cyril Simon Wedlund,[2] Christopher J. Mertens,[1] Mathieu Barthélemy,[3] Robert J. Lillis,[4] and Olivier Witasse[5]

Received 28 October 2011; revised 14 March 2012; accepted 19 March 2012; published 8 May 2012.

[1] One of the objectives of spectrometers onboard space missions is to retrieve atmospheric parameters (notably density, composition and temperature). To fulfill this objective, comparisons between observations and model results are necessary. Knowledge of these model uncertainties is therefore necessary, although usually not considered, to estimate the accuracy in planetary upper atmosphere remote sensing of these parameters. In Part I of this study, "Computing uncertainties in ionosphere-airglow models: I. Electron flux and species production uncertainties for Mars" (Gronoff et al., 2012), we presented the uncertainties in the production of excited states and ionized species from photon and electron impacts, computed with a Monte-Carlo approach, and we applied this technique to the Martian upper atmosphere. In the present paper, we present the results of propagation of these production errors to the main UV emissions and the study of other sources of uncertainties. As an example, we studied several aspects of the model uncertainties in the thermosphere of Mars, and especially the O(^{1}S) green line (557.7 nm, with its equivalent, the trans-auroral line at 297.2 nm), the Cameron bands CO($a^3\Pi$), and $CO_2^+(B^2\Sigma_u^+)$ doublet emissions. We first show that the excited species at the origin of these emissions are mainly produced by electron and photon impact. We demonstrate that it is possible to reduce the computation time by decoupling the different sources of uncertainties; moreover, we show that emission uncertainties can be large (>30%) because of the strong sensitivity to the production uncertainties. Our study demonstrates that uncertainty calculations are a crucial step prior to performing remote sensing in the atmosphere of Mars and the other planets and can be used as a guide to subsequent adjustments of cross sections based on aeronomical observations. Finally, we compare the simulations with observations from the SPICAM spectrometer on the Mars Express spacecraft. The production of excited species at the origin of the green line, the CO Cameron bands and the CO_2^+(B) doublet is found to be on the dayside, consistent with photon and electron impact on CO_2 as the main source of excitation of the three emissions, in contrast to the findings of Huestis et al. (2010) for the O(^{1}S) case. Moreover, we re-examine the cross section for the production of the Cameron bands by electron impact on CO_2.

Citation: Gronoff, G., C. Simon Wedlund, C. J. Mertens, M. Barthélemy, R. J. Lillis, and O. Witasse (2012), Computing uncertainties in ionosphere-airglow models: II. The Martian airglow, *J. Geophys. Res.*, *117*, A05309, doi:10.1029/2011JA017308.

[1]Chemistry and Dynamics Branch, Science Directorate, NASA Langley Research Center, Hampton, Virginia, USA.
[2]Belgian Institute for Space Aeronomy, Brussels, Belgium.
[3]Institut de Planétologie et d'Astrophysique de Grenoble, Grenoble, France.
[4]Space Sciences Laboratory, University of California Berkeley, Berkeley, California, USA.
[5]European Space Research and Technology Centre, European Space Agency, Noordwijk, Netherlands.

Corresponding author: G. Gronoff, Chemistry and Dynamics Branch, Science Directorate, NASA Langley Research Center, Mail Stop 401B, 21 Langley Blvd., Hampton, VA 23681-2199, USA. (guillaume.p.gronoff@nasa.gov)

0148-0227/12/2011JA017308

1. Introduction

[2] In the first part of this study ("Computing uncertainties in ionosphere-airglow models: I. Electron flux and species production uncertainties" [*Gronoff et al.*, 2012]), we described a typical ionization-airglow model called *Aeroplanets* and computed the excited state (including ions) species production uncertainties in the atmosphere of Mars. We explained the importance of computing forward model uncertainties for estimating the accuracy of our retrievals, for the improvement of the models, and for the design of future missions.

[3] In the present paper, we study in depth the main observed quantities for remote sensing: the emissions

(emission lines and bands) and how uncertainties are propagating in airglow models such as *Aeroplanets.*

[4] For the study of the Earth's atmosphere, it is always possible to send a rocket to calibrate the emission model [*McDade et al.*, 1986; *Murtagh et al.*, 1990]. However, this scheme is hardly reproducible for other planetary atmospheres. The estimation of the uncertainties in the emission process is therefore more crucial and must be done *before* the selection of emission lines for the remote sensing. This can be achieved by a thorough theoretical and statistical investigation, which is presented here.

[5] As an illustration, we examine three important emissions for the atmosphere of Mars:

[6] 1. The two forbidden lines arising from the $O(^1S)$ and $O(^1D)$ state transitions (the so-called green and red lines). The green line ($O(^1D - {}^1S)$, at 557.7 nm) and the trans-auroral line ($O(^3P - {}^1S)$, at 297.2 nm) arise from the same excited state $O(^1S)$, and are therefore proportional to each other. In the Martian dayglow, they are mainly excited by photon and electron impact on CO_2 (see discussion in section 4), and may be used to retrieve the density of this species. The red line ($O(^3P - {}^1D)$ triplet at 630.0, 636.4, 639.2 nm) arises from the $O(^1D)$ state, which, as $O(^1S)$, results from the dissociation of CO_2. This state is also excited by cascade from the $O(^1S)$ state, and from O_2^+ dissociative recombination. In the upper layers of the atmosphere, it is also excited by electron impact on O. This state is very sensitive to several parameters. One of the possible uses in remote sensing is the validation of the whole atmospheric parameters inversion; it could also be used to invert the O_2^+/e^- density in the main ionospheric layers of Mars by taking into account the approximation that these densities are equal.

[7] 2. The forbidden $CO(a^3\Pi - X^1\Sigma^+)$ Cameron bands, emitted in the 160–270 nm range, arise mainly from the dissociation of CO_2. These bands are very intense, and could be useful for the inversion of the CO_2 density. In practice, the extraction of these band intensities from the observed spectra may induce fitting uncertainties. Because the Cameron bands are quite intense, they have a high signal to noise (S/N) ratio when integrated. When fitting uncertainties become large, the S/N ratio of the Cameron bands is significantly degraded.

[8] 3. The $CO_2^+(B^2\Sigma_u^+ - X^2\Pi_g)$ doublet at 288.3–289.6 nm, which is allowed, but with negligible scattering (resonant or not: the density of the ground state, $CO_2^+(X)$, is negligible and therefore the resonant scattering; the CO_2 absorption cross section is below 10^{-25} cm^2 for that emission, which prevents large absorption and nonresonant scattering) for limb studies. It comes from the ionization of CO_2, and can be used to retrieve the density of that species.

[9] In section 2 we review the physical processes at the origin of the airglow, and we highlight the possible sources of uncertainties. In section 3 we present several emissions in the atmosphere of Mars that can be used for remote sensing. We detail the parameters (cross sections, reaction rates, etc) associated with the production and the loss of the excited state species, and with the emission. Moreover, we make a review of these parameters' uncertainties, and of the possible missing sources and sinks. In section 4 we study in depth the $O(^1S)$ sources and sinks, which are largely debated in the community. We show that the Mars Express' SPICAM instrument observations are compatible with CO_2 photodissociation as the main source of $O(^1S)$. In section 5 we compute the uncertainties for the case of Mars, and we summarize how to compute efficiently these uncertainties. In section 6 we discuss the effect of these uncertainties computation on the emissions selection for the retrieval purposes.

2. Species Density and the Emissions

[10] Electron transport models, such as *Aeroplanets*, can compute the productions of excited state species, including their uncertainties [*Gronoff et al.*, 2012]. However, these productions are not observable in a direct way: when in-situ measurements are not available, radiative transitions of the excited state species are the next-best observable.

[11] When an excited state species has a short chemical lifetime in the ionosphere/thermosphere (from below a second to a couple of minutes), the computation of the corresponding species density is relatively easy: a photochemical equilibrium can be assumed, and therefore it is not necessary to account for transport processes. Such computations compare generally well with experiments [*Gronoff et al.*, 2007]. On the other hand, the modeling of long-lived excited state and ionized species, such as $O^+(^4S)$ (ground state) and $O_2^+(X)$ in the ionosphere of Mars and Venus, can be extremely difficult. Such species, produced either by direct ionization, or by charge exchange and/or similar reactions, undergo several types of transport (ambipolar and eddy diffusion, thermospheric winds, etc). Their density in the ionosphere is thus extremely dependent on their initial concentration. This initial condition is fundamental in models, but is also of importance in the actual ionosphere, for example when it responds to a solar flare. A global circulation model (GCM, in the present case with thermospheric-ionospheric capabilities) study is sometimes needed to understand the observations [*Fox*, 2009; *Blelly et al.*, 2005]. The determination of the accuracy of a production model from the observation of these long-lived species (by in-situ measurement or emission) may then be challenging or even impossible. In practice, deriving production rates from densities might be achieved with in-situ measurements, which could be used in turn to retrieve the different species without any inversion from the production. Such in-situ measurements may significantly reduce the designed lifetime of a space mission: indeed, because the satellite plunges in regions of higher atmospheric densities, it must use extra fuel to sustain its orbit.

[12] As a consequence, for long-duration missions, an alternative method that has proved its reliability makes use of the other observable related to the production, that is, the emission [*Meier*, 1991; *Mertens et al.*, 2009]. Emissions come from the transitions between two states of the excited species, which can be divided into two kinds of transitions, either allowed or forbidden by the electric dipole transition selection rules. For forbidden transitions, the species is produced in a metastable state, and in a majority of cases the finite lifetime allows the computation of the state density in the photochemical approximation. The auto-absorption is negligible for forbidden transitions, so the computation of the emission does not depend on the intensity of the radiation at the transition wavelength (in some very rare cases,

Table 1. The $N_2(A^3\Sigma_u^+)$ Quenching Parameters for the Main Species in Planetary Atmospheres[a]

Reaction	Reaction Rate	Reference	Remarks
$N_2(A^3\Sigma_u^+) + O_2 \rightarrow O_2 + N_2$	$2.5 \times 10^{-12}(\pm 20\%)$	*Herron* [1999]	
$N_2(A^3\Sigma_u^+) + CO \rightarrow CO + N_2$	$1.6 \times 10^{-12}(\pm 30\%)$	*Herron* [1999]	
$N_2(A^3\Sigma_u^+) + CO_2 \rightarrow CO_2 + N_2$	$9.9 \pm 1.1 \times 10^{-15}$	*Dreyer et al.* [1974]	
$N_2(A^3\Sigma_u^+) + O \rightarrow O(\text{or } O(^1S)) + N_2$	$3.2 \pm 0.8 \times 10^{-11}\sqrt{T/298}$	*Hill et al.* [2000]	$O(^1S)$ yield : 0.47 ± 0.17
$N_2(A^3\Sigma_u^+) \rightarrow N_2 + h\nu_{\text{Vegard-Kaplan}}$	$A = 1/2.37\text{s}^{-1}(\pm 10\%)$	*Piper* [1993]	Dependence on the vibrations Unc. Est.

[a]These parameters are necessary for the $O(^1S)$ density computation and the Vegard-Kaplan emission computation. T is the neutral temperature. Unc. Est. stands for "uncertainty estimated."

inversions of population and MASER emission can be observed in the IR, for instance in the mesosphere of Mars and Venus for the CO_2 emission at 10 μm, the so-called LASER-band [*López-Puertas and Taylor*, 2001]). The volume emission rate then simply corresponds to the Einstein coefficient multiplied by the density of the excited state. The red and green lines of atomic oxygen are examples of forbidden transitions; the computation of their production is straightforward since no complex radiative transfer model is needed thanks to the excellent transmission of visible radiation through planetary upper atmospheres. On the other hand, the computation of the state density can be difficult since the chemical reaction rates have to be known.

[13] For allowed transitions, there are no density computation issues (even though the temperature can efficiently populate the upper state population: a Maxwellian distribution is accurate enough to account for that effect), but the auto-absorption can be important so that the optical depth may be large ($\tau > 1$). In this case, a radiative transfer model, taking into account multiple scattering and frequency redistribution is likely to be necessary [*Parkinson*, 2002; *Barthélemy et al.*, 2004].

[14] For the present study, a simple model was used (simple absorption, no resonant-scattering), which is sufficient for the most intense lines of the Martian UV spectrum. Under these assumptions, more complex emission lines like $O(^3S)$ emitting at 130.4 nm cannot be modeled [*Barthélemy et al.*, 2010].

3. The Emission Uncertainties Sources

[15] The radiance produced in a given transition can be computed when the production of the corresponding excited state species is known. But this modeling depends on several parameters, very specific to each state (losses due to quenching and radiative de-excitation) and transition (Einstein coefficient, resonant scattering, frequency redistribution, absorption of the radiation by the other species), producing numerous uncertainties. In the following subsections, we review the processes at the origin of some of the most intense emissions in the Martian dayglow.

3.1. The Case of $O(^1S)$ and $O(^1D)$

[16] The $O(^1S)$ and $O(^1D)$ states have lifetimes of the order of a second to a couple of minutes. $O(^3P - {}^1D)$, $O(^1D - {}^1S)$, and $O(^3P - {}^1S)$ are forbidden transitions. It is possible to use a photochemical equilibrium approximation to compute the density of these states when the nature of the sources and sinks is known. When the Einstein coefficients are known, the computed density may be used to calculate the intensities of the emissions.

[17] Several sources for the reaction rates and the Einstein coefficients are available, especially online; see notably the National Institute of Standards and Technology (NIST) Atomic Spectra Database (http://physics.nist.gov/asd [*Ralchenko et al.*, 2010]), the JPL Chemical Kinetics and Photochemical Data for Use in Atmospheric Studies site (http://jpldataeval.jpl.nasa.gov/download.html), the IUPAC Subcommittee on Gas Kinetic Data Evaluation site (http://www.iupac-kinetic.ch.cam.ac.uk/ [*Atkinson et al.*, 2004]), *Dunlea and Ravishankara* [2004], and the Kinetic Database for Astrochemistry (http://kida.obs.u-bordeaux1.fr). In Tables 1–5, the notation "uncertainty estimated" (Unc. Est.) indicates that we could not provide any uncertainty for the given reaction rate, and that we therefore had to estimate one. Such estimates are based on the uncertainties for similar reactions and, when

Table 2. The $O(^1S)$ Quenching Parameters for the Main Species in the Martian Atmosphere[a]

Reaction	Reaction Rate (Default: $\text{cm}^3\ \text{s}^{-1}$)	Reference	Remarks
$O(^1S) \rightarrow O(^1D) + h\nu_{557.734\text{nm}}$	$1.26\ \text{s}^{-1} \pm 25\%$	NIST	Problem with the 5577/2972 ratio *Slanger et al.* [2006b]
$O(^1S) \rightarrow O(^3P) + h\nu_{297.229\text{nm}}$	$7.54 \times 10^{-2}\ \text{s}^{-1} \pm 25\%$	NIST	Unc. Est. 25% (See text.)
$O(^1S) + O_2 \rightarrow O\|O(^1D) + O_2$	$2.32 \pm 0.94 \times 10^{-12}\exp\left(-\frac{812}{T}\right)$	*Capetanakis et al.* [1993]	Branching ratio in *Fox and Sung* [2001] 31% $O(^1D)$, 69% $O(^3P)$
$O(^1S) + CO_2 \rightarrow O\|O(^1D) + CO_2$	$3.21 \pm 0.25 \times 10^{-11}\exp\left(-\frac{1323}{T}\right)$	*Capetanakis et al.* [1993]	63% $O(^1D)$, 37% $O(^3P)$
$O(^1S) + CO \rightarrow CO + O(^1D)$ (?)	$7.40 \pm 0.48 \times 10^{-14}\exp\left(-\frac{957}{T}\right)$	*Capetanakis et al.* [1993]	*Fox and Sung* [2001] for $O(^1D)$
$O(^1S) + O2(a^1\Delta_g)$	$1.7 \pm 0.3 \times 10^{-10}$	*Slanger and Black* [1981]	Very important compared to the CO_2 quenching. 17% $O(^1D)$+O2($b^1\Sigma_g^+$) 19% dissociation
$O(^1S) + O \rightarrow O(^1D)$	$1.2 \times 10^{-14} \pm 50\%$	*Krauss and Neumann* [1975]	Unc. Est.
		Slanger and Black [1981]	Theoretical computation.
$O(^1S) + N_2 \rightarrow O(^1D)$	$2 \times 10^{-17} \pm 50\%$	*Atkinson and Welge* [1972]	Induced emission. Negligible. Unc. Est.
$O(^1S) + e \rightarrow O(^1D)$	$8.5 \times 10^{-9} \pm 50\%$	*Berrington and Burke* [1981]	Theoretical work. Unc. Est.
$O(^1S) + e \rightarrow O(^3P)$	$1.56 \times 10^{-10}\left(\frac{Te}{300}\right)^{0.94} \pm 50\%$	*Berrington and Burke* [1981]	Theoretical work. Unc. Est.

[a]Some of these reactions produce $O(^1D)$ and therefore are needed for the computation of the emissions of that species. T is the neutral temperature, and Te the electron temperature.

Table 3. The O(^{1}S) Production Through Cascade and Chemical Reactions[a]

Reaction	Reaction Rate (Default: cm^3 s^{-1})	Reference	Remarks
$O_2^+ + e \rightarrow O(^1S)$	*Te* dependence 40%	*Kella et al.* [1997]; *Fox and Sung* [2001]	See text; strong influence of vibrational status of O_2^+.
$N_2(A^3\Sigma_u^+) + O \rightarrow O(^1S) + N_2$	$1.4 \pm 0.6 \times 10^{-11}\sqrt{T/298}$	*Herron* [1999]	See Table 1.
$O_2^+ + N \rightarrow NO^+ + O(^1S)$	$2.25 \times 10^{-11} \pm 50$ %	*Frederick et al.* [1976]; *Kopp et al.* [1977]	See text and *Gronoff et al.* [2008].
$O + O + M \rightarrow O_2^* + M$	Empirical ratio	*Barth and Hildebrandt* [1961]	Barth mechanism.
$O_2^* + O \rightarrow O(^1S) + O_2$	Empirical ratio		See also *Gronoff et al.* [2008].

[a]Note that some of these reactions are still uncertain, as discussed in the text and in the references. For the Barth mechanism, no actual reaction rate exists, but an empirical parameterization has been done [*McDade et al.*, 1986; *Murtagh et al.*, 1990; *Gronoff et al.*, 2008]. *T* is the neutral temperature, and *Te* the electron temperature.

possible, on the typical variations between the different sources for the reaction rate.

3.1.1. O(^{1}S)

[18] This metastable state has transitions to the O(^{1}D) state, at 557.7 nm and to the O(^{3}P) state, at 297.2 nm. Some uncertainties still exist concerning the value of these transitions' Einstein coefficients, and for the existence of some O(^{1}S) sources which appear to be non-negligible for nighttime conditions. At Mars, in the dayside, the main sources of O(^{1}S) are the photodissociation of CO_2 and the dissociative recombination of O_2^+. The proportion of the latter source in the total emission is still debated, and in Figure 1, this source production has been plotted following several hypotheses on its efficiency. This problem will be discussed in depth in section 4.

3.1.2. O(^{1}D)

[19] This metastable state emits the 630 nm triplet when it transits to the oxygen ground state. The non-physical sources are listed in Table 2 and 4 for the productions due to the quenching of O(^{1}S). The quenching processes are listed in Table 5. The longer lifetime of these states, of the order of 100 s, implies an important sensitivity to quenching processes. Such sensitivity can be useful for remote sensing applications: the model-observation comparison can be treated as a quality test for the deduced atmosphere.

3.2. The Cameron Bands and the CO_2^+ Doublet

[20] The Cameron bands arise from the transition of the CO(a$^3\Pi$) state to the ground state [*Conway*, 1981]. This is a metastable state, but with a 3.16 ms radiative lifetime. In upper atmospheres, this lifetime prevents any quenching reaction from being efficient; this transition can be treated as allowed (no need to compute the density) but without the need for a complex radiative transfer model including the resonant scattering of the solar source.

[21] For this transition, one difficulty arises from the possibility of production due to the dissociative recombination of CO_2^+ [*Skrzypkowski et al.*, 1998]. Another difficulty emerges from the wavelength distribution of the transition in the 180–250 nm range: the absorption by CO_2 is not negligible below 200 nm, and therefore limb observations are affected [*Gronoff et al.*, 2010]. The main problem for this emission is uncertainty in the cross section for the CO(a$^3\Pi$) production from electron impact on CO_2. This cross section was initially measured by *Ajello* [1971] but was later reevaluated by *Erdman and Zipf* [1983]. The cross section at 80 eV was first evaluated at 1.0 10^{-17} cm^{-2}. It was multiplied by a factor of 9 because of reconsideration of the radiative lifetime, and subsequently multiplied by a factor of 2.7 because the CO(a$^3\Pi$) molecules were observed to be faster and might escape detection [*Wells et al.*, 1972]. Therefore, the value reported by *Avakyan et al.* [1998] is 2.4 10^{-16} cm^{-2} at 80 eV, and the correction has been applied for all the energies. Such a correction was known to be too high to account for the observed Cameron bands at Mars [*Erdman and Zipf*, 1983], and the newly reevaluated cross section was divided by 2 in *Simon et al.* [2009], *Cox et al.* [2010], and *Jain and Bhardwaj* [2011b]. The recent experimental and theoretical work by *Gilijamse et al.* [2007] re-analyzed the radiative lifetime of CO(a$^3\Pi$), and found a value of 3.16 ms, which is 3 times less than the value of [*Johnson*, 1972] used previously to correct the cross sections. Therefore, the cross section reported by *Avakyan et al.* [1998] should be divided by 3 in light of these new measurements, giving a value of 0.8 10^{-16} cm^{-2} at 80 eV. In the following, this corrected cross section will be used. A 25% uncertainty is estimated for these re-calibrated data. The data-model comparison in section 5.3 shows that this correction is supported by the observations and should be used as reference for future studies.

[22] The CO_2^+ doublet is an allowed transition. It comes from the CO_2^+(B) excited state transiting to the ground state. Since CO_2^+ densities are typically low in planetary atmospheres (this ion easily reacts to form O_2^+ [*Withers*, 2009]), the resonant scattering is negligible [*Fox and Bougher*, 1991]. Because the doublet is emitted at 289 nm, therefore with a low absorption, the computation of this transition should be modeled more accurately and completely than

Table 4. The O(^{1}D) Production Through Cascade and Chemical Reactions[a]

Reaction	Reaction Rate (Default: cm^3 s^{-1})	Reference	Remarks
$O_2^+ + e \rightarrow O(^1D)$	*Te* dependence 14%	*Kella et al.* [1997]	The reaction depends on *Te*; see text.
$O + e \rightarrow O(^1D)$	*Te* dependence 20% est	*Mantas* [1994]	See text; Unc. Est. following *Doering* [1992].
$N^+ + O_2 \rightarrow O(^1D)$	$1.8 \times 10^{-10} \pm 50\%$	*Langford et al.* [1986]	See also *Huntress and Anicich* [1976].
$N(^2D) + O_2 \rightarrow O(^1D)$	$5 \times 10^{-12} \pm 100\%$	*Rawlins et al.* [1989]	Discussion in *Link and Swaminathan* [1992]: could be 0.
$CO^+ + e \rightarrow O(^1D)$	$2.5 \times 10^{-6}\left(\frac{300}{Te}\right)^{0.55} \pm 15\%$	*Rosén et al.* [1998]	Unc. Est.

[a]Note that some of these reactions are still uncertain, as discussed in the text and in the references. *Te* is the electron temperature.

Table 5. The O(^{1}D) Quenching Parameters for the Main Species in the Martian Atmosphere[a]

Reaction	Reaction Rate (Default: cm^3 s^{-1})	Reference	Remarks
$O(^1D) \rightarrow O(^3P) + 630.0304nm$	$5.63 \times 10^{-3} \pm 20\%$ s^{-1}	NIST	Unc. Est.
$O(^1D) \rightarrow O(^3P) + 636.3776nm$	$1.82 \times 10^{-3} \pm 50\%$ s^{-1}	NIST	Unc. Est.
$O(^1D) \rightarrow O(^3P) + 639.1733nm$	$8.60 \times 10^{-7} \pm 30\%$ s^{-1}	NIST	Unc. Est.
$O(^1D) + O_2 \rightarrow O + O_2$	$3.3 \times 10^{-11} \exp\frac{55}{T} \pm 10\%$	JPL	Uncertainty at 300 K; it is possible to use a formula for T dependence.
$O(^1D) + O \rightarrow 2O$	$2.2 \pm 0.3 \times 10^{-11}$	*Kalogerakis et al.* [2009]	Constant: 2.5 in the upper atmosphere (T dependence).
$O(^1D) + N_2 \rightarrow O + N_2$	$2.5 \times 10^{-11} \exp\frac{110}{T} \pm 10\%$	JPL	Creation of N_2O: 1E-36, neglected
$O(^1D) + CO_2 \rightarrow O + CO_2$	$7.5 \times 10^{-11} \exp\frac{115}{T} \pm 15\%$	JPL	
$O(^1D) + CO \rightarrow O + CO(CO_2?)$	$3.6 \times 10^{-11} \pm 14\%$	*Schofield* [1978]	Creation of CO_2?
$O(^1D) + e \rightarrow O$	$2.87 \times 10^{-10} \left(\frac{Te}{300}\right)^{0.91} \pm 50\%$	*Berrington and Burke* [1981]	Theoretical work; Unc. Est.

[a] T is the neutral temperature, and Te the electron temperature.

O(^{1}S), which has chemical contributions in its production, and the Cameron bands, which are absorbed.

4. The O(^{1}S) Sources and Sinks

[23] The sources and sinks of O(^{1}S) in planetary atmospheres have been largely debated. The observations at Mars and Venus allow us to highlight the different problems associated with the green and transauroral line modeling.

4.1. The $N_2(A^3\Sigma_u^+)$ Source of O(^{1}S)

[24] *Herron* [1999] evaluated the reaction rate for several reactions including N_2 from experiments. It is reported that the reaction $N_2(A^3\Sigma_u^+)$ + O can yield O(^{1}S) with a non-negligible rate. For some conditions, it is important to evaluate the density of that excited species to compute the O(^{1}S) density and transitions [*Witasse et al.*, 1999; *Culot et al.*, 2005]. The sink reactions are listed in Table 1, along with the associated rates, uncertainties, and chemical sources. The productions of $N_2(A^3\Sigma_u^+)$ come mainly from the electron

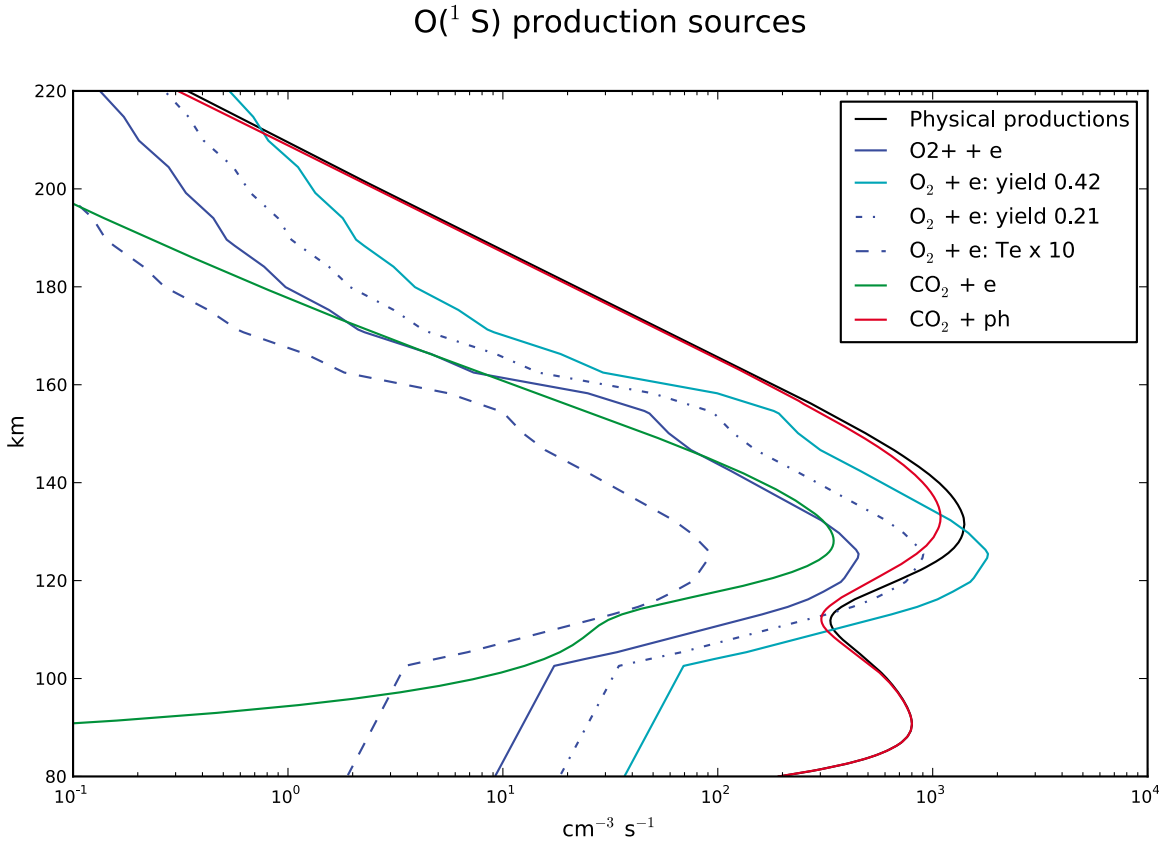

Figure 1. The detailed production of O(^{1}S) and the sensitivity study for the reaction O_2^+ + e. The main source of O(^{1}S) is the photodissociation of CO_2. For the dissociative recombination of O_2^+ to be of the order of the photodissociation, the O(^{1}S) yield of the recombination should be 0.42. The observation of the low altitude peak (below 100 km altitude), produced by the photodissociation of CO_2 by the solar Ly$_\alpha$ radiation, would be a further argument in favor of a CO_2 photodissociative source for O(^{1}S).

impact on N_2, for which cross sections are present in the *AtMoCiad* database [*Gronoff et al.*, 2012]. Since the radiative de-excitation of that excited state emits the Vegard-Kaplan bands, it is possible to estimate the magnitude of the error by observing these bands if we do not compute this reaction. *Jain and Bhardwaj* [2011a] have compared their model and the SPICAM data for these bands at Mars, concluding that current models overestimate the N_2 density in the atmosphere. Therefore, $N_2(A^3\Sigma_u^+)$ is a negligible source of $O(^1S)$ for that planet.

4.2. The Barth Mechanism

[25] The question of the main nightside source for $O(^1S)$ is not yet solved for CO_2-rich atmospheres. At Earth, the Barth mechanism, which consists of a three O recombination with a catalyzer and an undetermined O_2^* intermediate excited state ($O + O + M \rightarrow O_2^* + M$; $O_2^* + O \rightarrow O_2 + O(^1S)$), is known to be the main mechanism in non-auroral regions. But the efficiency at planets like Venus is questionable [*Gronoff et al.*, 2008]. Recently, *García Muñoz et al.* [2009] reported that with their level of sensitivity, it had not been possible to detect the green line in the nightside mesosphere of Venus with the VIRTIS instrument aboard Venus Express. From this perspective, the green line may be of thermospheric origin, and the $O_2^+ + N \rightarrow NO^+ + O(^1S)$ reaction is a good candidate (even though it is not spin-allowed, see *Gronoff et al.* [2008]). The observation of sporadic nighttime ionospheres by VERA [*Pätzold et al.*, 2007] shows that such nighttime ion chemistry can occur below 200 km. The sporadic behavior of this effect is compatible with the extreme variability of this emission in the Venusian nightglow [*Slanger et al.*, 2001, 2006a]. If the precursor of the Barth mechanism, O_2^*, is the $O_2(c^1\Sigma_u^-)$ state as suggested by some teams [e.g., *Snively et al.*, 2010], then the very small intensity of the emissions from this state observed at Venus [*Parisot*, 1986] is another argument in favor of a thermospheric emission.

4.3. The O_2^+ Dissociative Recombination

4.3.1. The Effects of the Dissociative Recombination

[26] Another problem arises from the $O_2^+ + e$ reaction. This reaction, very exothermic, is probably at the origin of the suprathermal oxygen in the Martian atmosphere [*Chaufray et al.*, 2009]. But it does not seem sufficient to account for the hot oxygen observed at Mars with the UV spectrometer SPICAM aboard Mars Express. Other studies suggest that this hot oxygen does not exist in the large quantities reported with SPICAM [*Feldman et al.*, 2010, 2011]. The cause of the discrepancy between these two observations is probably a misinterpretation of the data coming from the overlapping of the $CO(a^1\Pi)$ fourth positive bands with the $O(^3S)$ 130.4 nm transition observed by SPICAM (*Feldman et al.* [1976]; *Kassal* [1975, 1976]; *Durrance* [1981]; *Barthélemy et al.* [2010]; M. Barthélemy et al., The radiative transfer problem of the O I 130-nm triplet in planetary atmospheres, in preparation, 2012): the absorption of the 130.4 nm radiation by CO at the altitudes below 150 km modifies the shape of the retrieved O profile that is subsequently interpreted in terms of hot oxygen. Therefore, we should be very careful about the different constraints put on the $O_2^+ + e$ reaction efficiency by these observations. Moreover, the theoretical and laboratory experiments tend to show a strong influence of the kinetic temperature and the vibrational state of O_2^+ on the reaction rate and products. The most used reaction rate for the recombination is the *Mehr and Biondi* [1969] one, with the *Kella et al.* [1997] branching ratio for the production of hot oxygen, $O(^1S)$ and $O(^1D)$:

$$k_{O_2^+ + e^-} = 1.95 \times 10^{-7} \left(\frac{300}{T_e}\right)^{0.7} \pm 10\% \; T_e < 1200\text{K} \quad (1)$$

$$k_{O_2^+ + e^-} = 7.38 \times 10^{-7} \left(\frac{1200}{T_e}\right)^{0.56} \pm 10\% \; T_e > 1200\text{K} \quad (2)$$

The yield of $O(^3P)$ is 0.86 ± 0.15, the one of $O(^1D)$ is 1.09 ± 0.15, and for $O(^1S)$ it is 0.05 ± 0.02. These values are widely used in the community [see for instance *Valeille et al.*, 2010]. Anyway, recent measurements [*Peverall et al.*, 2000, 2001] suggest that the reaction rate value should be increased (2.4 instead of 1.95).

4.3.2. Sensitivity Study of the O_2^+ Importance in the $O(^1S)$ Production

[27] In *Huestis et al.* [2010], it is suggested that the dissociative recombination of O_2^+ accounts for the major part of the $O(^1S)$ production in the atmosphere of Mars. In Figure 1, the different parameters that affect the O_2^+ recombination efficiency and its $O(^1S)$ yield have been studied and compared with the physical source, i.e., the electron and photon impact on CO_2.

[28] The first unknown in the ionosphere of Mars is the electron temperature. This temperature must be greater than the neutral temperature, and is probably underestimated in the current models. The multiplication of that temperature by 10 reduces the efficiency of the O_2^+ recombination, and therefore cannot explain a higher $O(^1S)$ creation.

[29] Following *Petrignani et al.* [2004], *Huestis et al.* [2010] suggested that the vibrational level of O_2^+ could explain the high intensity of $O(^1S)$: the recombination of $O_2^+(\nu = 2)$ is much more efficient than the recombination of the ground state: it has a yield of 0.21 instead of 0.05, but the reaction rate for the recombination is divided by two. In the local thermodynamic equilibrium (LTE) approximation, only a few percent of the O_2^+ must be in that vibrational state, but non-LTE processes could increase this proportion. To constrain this hypothesis, we considered that all the O_2^+ in the ionosphere was in that vibrational state. In this condition, the $O(^1S)$ creation is still too low, but when we consider a 0.42 yield (which could be seen as a 0.21 yield without the reaction rate correction) the $O(^1S)$ creation from recombination becomes roughly equal to that from CO_2 dissociation. The conditions needed to reach the $O(^1S)$ production level are therefore extreme and unrealistic. If the recombination is the main source of $O(^1S)$, the O_2^+ density should therefore be much higher than that computed in the models.

4.3.3. Is O_2^+ Recombination the Main Source of $O(^1S)$ at Mars?

[30] Contrary to the suggestion of *Huestis et al.* [2010], the $O_2^+ + e$ reaction rate and the yield of $O(^1S)$ cannot explain the UV observation for the dayside of Mars, without considering the O_2^+ density to be much more important than observations suggest. The conclusions of *Huestis et al.* [2010], in contrast to previous modeling-data comparison studies of $O(^1S)$ at 297.2 nm [e.g., *Shematovich et al.*, 2008;

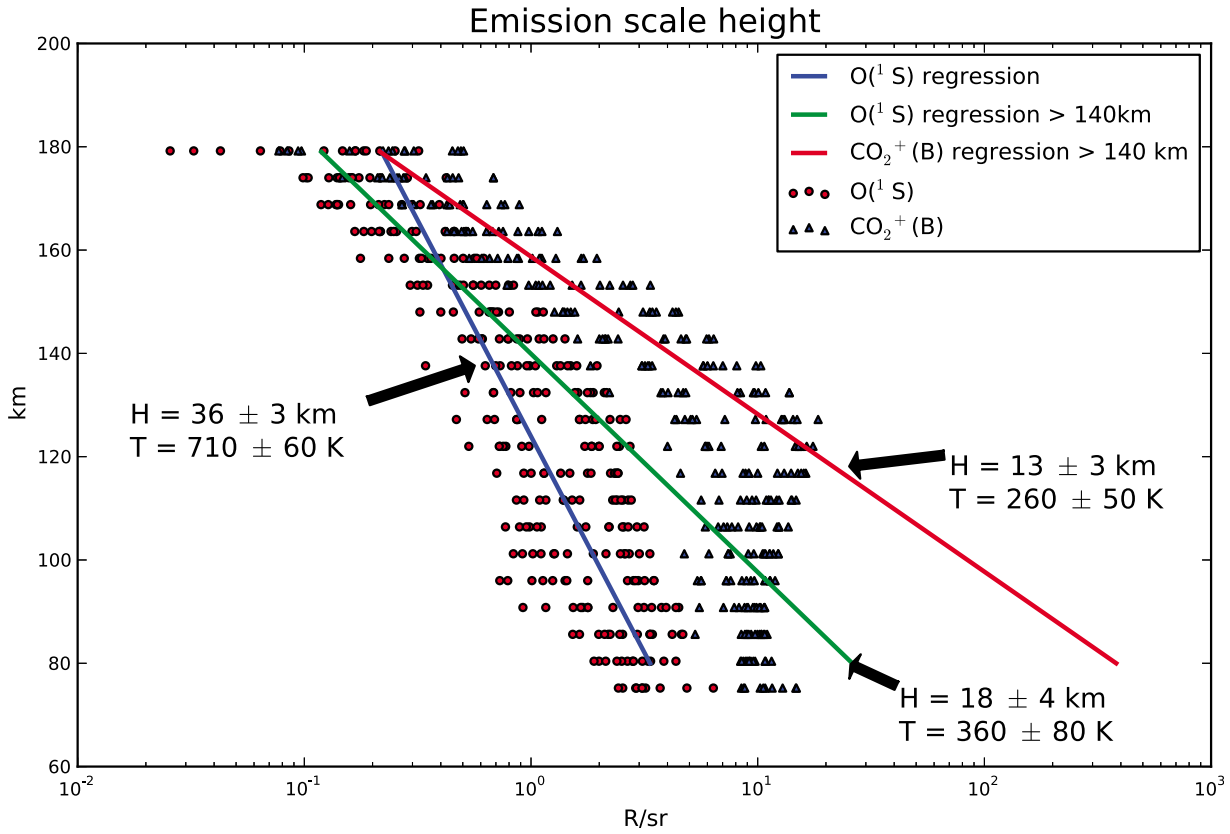

Figure 2. The scale height of the atmosphere deduced from the emissions of O(^{1}S) and CO_2^+(B). When the selected observations have similar parameters, it is possible to see that the scale height deduced from the data above the emissions peak are consistent.

Simon et al., 2009], suggest that the O_2^+ dissociative recombination is the main source of the O(^{1}S) state at Mars.

[31] These new developments, in order to be properly assessed, have motivated a critical reevaluation of available data comparison with theory and source/sink mechanisms (notably photodissociation of CO_2).

4.4. The CO_2 Photodissociation

[32] When taking into account the recommended cross section for O(^{1}S) production by CO_2 [*Gronoff et al.*, 2008; *Simon et al.*, 2009], the influence of the O_2^+ recombination on the O(^{1}S) production is negligible compared to the photodissociation of CO_2. Moreover, the observations of the Venusian airglow [*LeCompte et al.*, 1989] are in agreement with a significant photoproduction of O(^{1}S).

[33] The point that influenced the conclusion of *Huestis et al.* [2010] for the origin of O(^{1}S) was the deduced scale height of the 297.2 nm emission when all the SPICAM observations were taken into account: this scale height was significantly different from the ones observed for the Cameron bands and the CO_2^+(B) doublet. The observed discrepancy might be explained by the variations of the density of the Martian upper atmosphere, up to a factor of 20 [*Bougher et al.*, 2001; *Withers et al.*, 2003; *Bougher et al.*, 2004; *Cahoy et al.*, 2006, 2007; *Simon et al.*, 2009; *Forget et al.*, 2009], and the lower intensity of the 297.2 nm emission in comparison with the two other emissions (lower S/N ratio). The 947 orbit analyzed in *Huestis et al.* [2010] is also problematic because of solar contamination, the low signal to noise level for the 297.2 nm emission, including contamination by N_2 Vegard-Kaplan (0–9), and the large range of solar zenith angles.

[34] To assess these parameters, we re-analyzed the SPICAM data presented in *Simon et al.* [2009]: in Figure 2, we plotted the SPICAM data points for the 37 orbits of *Simon et al.* [2009], in order to reproduce the *Huestis et al.* [2010] analysis.

[35] The determination of the scale height was done using a linear regression. The interpretation in terms of temperature assumed a mean molar mass of 44.01 g/mol, which corresponds to the CO_2 molar mass. This interpretation implies that we neglect the absorption by the other species in the production of the emissions and in the radiative transfer. It also assumes a constant neutral temperature above the emission peak. For the CO_2^+(B) emission, the deduced scale height is 13 ± 3 km (260 ± 50 K), which is compatible with the scale height deduced from the O(^{1}S) emission above 140 km: 18 ± 4 km (360 ± 80 K). The uncertainties in our study are computed from the linear fit covariant matrix [*Bevington and Robinson*, 2003], by taking the standard deviation of the data at each altitude as the data uncertainty. These values are comparable to the deduced scale height of 12.3 ± 0.1 km of *Huestis et al.* [2010] from the CO_2^+(B) emission. In addition, the scale height deduced from the whole O(^{1}S) emission profile is 36 ± 3 km. This value does not agree well with the 25.3 ± 0.3 km value of *Huestis et al.*

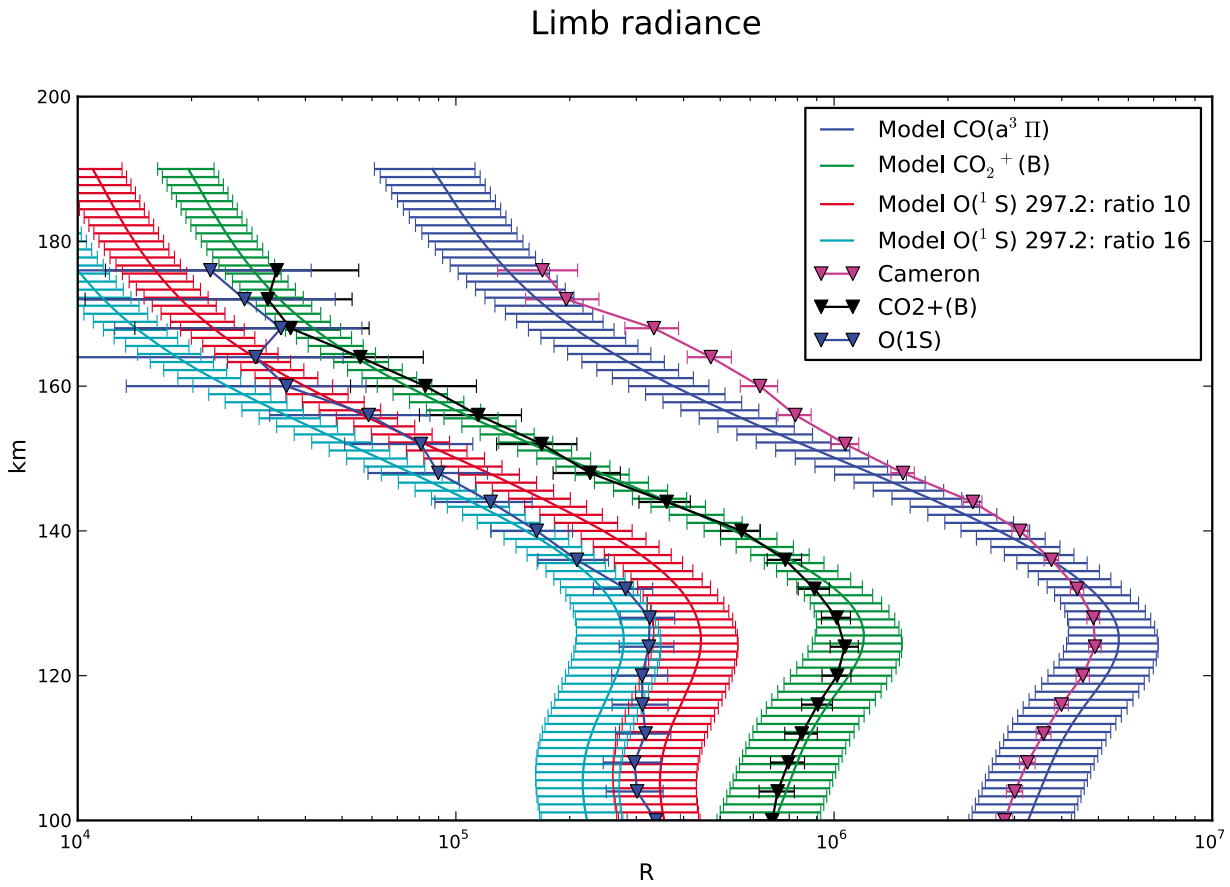

Figure 3. *Aeroplanets* modeling–SPICAM observation comparison. The O(^{1}S), CO_2^+(B), and Cameron bands limb radiances observations are compared with the model. The neutral atmosphere has been adapted to fit the CO_2^+(B) emission.

[2010] but shows that when all the data are taken into account, the scale height is significantly increased.

[36] The main difference between the datasets used in the *Huestis et al.* [2010] analysis and the present one concerns the selection of the orbit data. The present set takes into account only the data for which no contamination from solar light is observed, while the *Huestis et al.* [2010] work uses more orbits for which the solar contribution is subtracted below 90 km, without details on the technique. It unfortunately prevents us from analyzing why the uncertainties in the retrieval do not compare with our work. When the different orbits are analyzed one by one, and not plotted together, a peak is visible at about 120 km, with variations in altitude up to 20 km. This variation in altitude of the emission peak of O(^{1}S) is the same as the variations of the emission peaks of CO_2^+(B) and CO(a^{3}Π). These variations are correlated to that of the electron density peak, suggesting a common origin. Observations by the Mars Global Surveyor Radio Science Experiment showed that they originate from the neutral atmosphere variations [*Zou et al.*, 2011]. Therefore, when plotted together, these different orbits create a large variation in intensity below 140 km, hence the increase of the scale height when all the altitudes are taken into account. In addition, dayside exospheric temperatures can vary from 200 K to 400 K in the atmosphere of Mars [*Forbes et al.*, 2008], modifying the slope of the limb radiances [*Simon Wedlund et al.*, 2011].

[37] As a consequence, the use of all the data, like in *Huestis et al.* [2010], may alter the scale height retrieval and can be highly misleading on the processes at work. The O(^{1}S) emission at 297.2 nm present a clear peak around 120 km altitude when only one orbit is taken into account, or when a discrimination on the Martian solar longitude, the solar activity and zenith angle of the averaged data is done (preferred analysis).

[38] Figure 3 shows very good agreement between observations (data for orbit 1298, 21 January 2005, Ls = 148, F_{107} at Earth = 85, F_{107} at Mars = 35, SZA = 39) and the modeled emissions, based on the CO_2 photodissociation as the main source for O(^{1}S). This is in contradiction with the *Huestis et al.* [2010] hypothesis of an O(^{1}S) production due mainly to O_2^+ dissociative recombination and following a different scale height because of the O_2^+ profile. It is not possible to disciminate between a O_2^+ recombination creation of O(^{1}S) and a CO_2 photodissociation from the observations if the O_2^+ density slope follows the photodissociation slope. But the both chemical and observational evidences for this process are questionable, and the non-efficiency of the photodissociation process (the O_2^+ recombination was suggested to replace this process in *Huestis et al.* [2010]) would be left unexplained while it is consistent with the observations and the laboratory experiments. Therefore, our scale height study as well as our new simulations with *Aeroplanets* strongly

support that the recommended main source for $O(^1S)$ species on the dayside is the photodissociation of CO_2, not the O_2^+ recombination.

4.5. The Einstein Coefficient

[39] Concerning the Einstein coefficients, *Slanger et al.* [2006b] have suggested that the ratio of the 557.7/297.2 emissions should be 9.8 ± 1.0 instead of the NIST recommended value of 16.4. Recent observations with the OSIRIS spectrograph on the Odin spacecraft suggest a ratio of 9.3 ± 0.5 [*Gattinger et al.*, 2009]. The difficulties of these determinations come from the need for a good cross-calibration in both optical and UV channels, and from the necessity to remove the contamination by the overlapping N_2 Vegard-Kaplan bands. Unfortunately, the question of whether we should increase the 297.2-nm Einstein coefficient, decrease that of the 557.7-nm line, or do both is not answered in these papers. A first estimation of the needed modifications shows that an increase of 65% of the 297.2 coefficient, or a decrease of 40% of the 557.7 one are sufficient. If both are changed with the same relative amplitude, a modification of 25% for each line's Einstein coefficient is necessary. Unfortunately, if the radiative transition is the predominant source of de-excitation of $O(^1S)$ at the altitude considered (the others are negligible), the computation shows that the intensity modification between each case is of the order of 1% or less. Because of the $O(^1S)$ radiative lifetime, of the order of 0.7 s, the radiative transition is often predominant at the emission peak, and therefore no conclusion is possible concerning modifications to make (mathematically, in that case, the $O(^1S)$ density is equal to the production divided by the Einstein coefficient, and the emission is the density multiplied by the Einstein coefficient; the emission is therefore equal to the production, and the only information that can be derived from the observation is the ratio 297.2/557.7). In addition, we show in section 5.3.2 that the uncertainty in the emission, coming from the uncertainties in the chemical reaction rates and the excited state species production, is also of the order of 25% (this result is similar for the Earth's $O(^1S)$ emissions), which creates difficulties for the determination of the correction when the radiative de-excitation is not dominant. Nevertheless, with a good knowledge of the state of the atmosphere, the solar flux [*Dudok de Wit et al.*, 2005, 2008], and an accurate calibration of the green/UV line observations, it may be possible to give a first estimate of the correct values based on satellite observations. The importance of the model uncertainties implies that such an experiment would need an in-situ rocket measurement, and therefore the available data are not sufficient to solve this problem.

[40] In Table 2, we give the Einstein coefficients' NIST values without any correction, with an uncertainty estimated at 25%: the Einstein coefficients coming mainly from theoretical work, the uncertainties were not claimed; these uncertainties are consistent with the previous discussion. Nevertheless, if the theoretical works alone are taken into account and compared to each other, an uncertainty of 10% is better suited for the $^1D - {}^1S$ transition [*Baluja and Zeippen*, 1988], while the $^3P - {}^1S$ transition has a 25% uncertainty. This larger uncertainty in the theoretical work for the 297.2 nm transition indicates that the increase of the corresponding Einstein coefficient is the more probable solution to the observational problem. In Table 3, we present the non-physical production mechanism, i.e., not coming from photon or electron impact on atoms or molecules.

5. Computing the Emissions Uncertainties

5.1. Species Production Uncertainty

[41] The computation of the production uncertainties is independent of the emission uncertainties computation (a modification of the uncertainties parameter of the latter will not affect the former). To optimize the process, production uncertainties are computed independently in order to be used as a single parameter for the calculation of total uncertainties. These production uncertainties come mainly from the electron and photon impact cross section uncertainties [see *Gronoff et al.*, 2012].

[42] Figure 4 shows the production uncertainties for the excited states species at the origin of the different emissions for the Martian example. They have been computed for the same conditions and with the same technique as described in *Gronoff et al.* [2012] but without taking into account uncertainties coming from the solar flux. The cross sections and their uncertainties for the different production mechanisms come from the AtMoCiad database. The cross section uncertainty for the Cameron band emission from electron impact on CO_2 is discussed in section 5.3.4. For the computation of all the minor excited states, i.e., those for which even a large uncertainty does not affect the other productions through a modification of the incoming flux of particle, we can consider only one free parameter, which prevents an exponential multiplication of the Monte-Carlo runs.

[43] The main production peak for $CO_2^+(B)$, the Cameron bands, and $O(^1S)$, situated at 130 km altitude, occurs at the same altitude as the ion production peak. The uncertainties also increase below the ionization peak. However, for $O(^1S)$, a second peak is seen due to the photodissociation of CO_2 by the Ly_α photons from the Sun. For $O(^1D)$, which is efficiently produced by photons in the 100–200 nm wavelength range, the peak production occurs at about 80 km. At 10 km above the production peak—i.e., at 140 km—the uncertainty for the production of $O(^1S)$ and $CO_2^+(B)$ is about 20%. The $CO(a^3\Pi)$ uncertainty is higher at these altitudes, between 30% and 40%, and the $O(^1D)$ production uncertainty is about 30% below 160 km and slightly increases above.

5.2. Emission Uncertainties

[44] The two components of interest for the emissions are the volume emission rate (VER) and the limb radiance (LR). The former corresponds to the emission of photons per unit volume per second while the latter corresponds to the intensity measured by a satellite observing at the limb. The VER is defined with the altitude of the emitting unit volume considered, and the point where the line of sight is tangent to the planet defines the LR altitude. The evaluation of the LR uncertainties allows us to define the minimal accuracy for a remote sensing system because it should be limited by the model uncertainties, and not those of the observation. The VER, which can be derived from the observations using an Abel inversion, is more directly related to the model (no integration along the line of sight) and is better suited to estimate and compute the uncertainties for the retrieval.

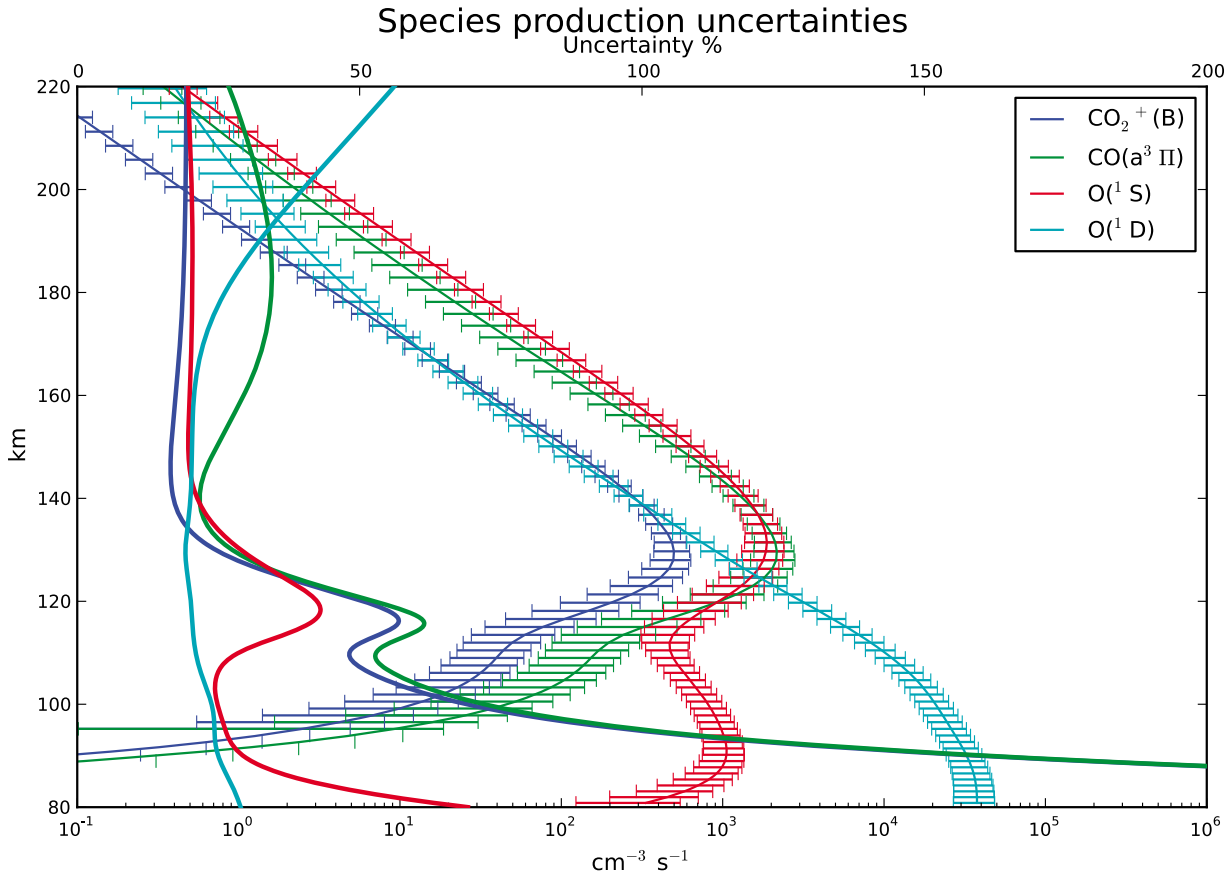

Figure 4. Uncertainties for the production of the emitting species, computed with *Aeroplanets*. The detailed technique is described in *Gronoff et al.* [2012]. The line with error bars corresponds to the computed production with the uncertainties, and the solid lines correspond to the corresponding percentage of uncertainty.

[45] When the VER uncertainties are computed, it is possible to consider each altitude as independent. Therefore, the number of free parameters, which determines the minimum number of Monte-Carlo simulations to perform [*Gronoff et al.*, 2012], is equal to the number of chemical reactions needed plus one corresponding to the species production uncertainty (when several independent emissions are computed at the same time, the number of free parameters stands for the maximum number of chemical reactions needed). This scenario cannot be adapted for the LR case: the integration along the path corresponds to an integration along several altitudes. If we continue to consider each VER altitude as independent before the computation, the number of free parameters will increase dramatically (we add the altitudes to the previous free parameters), and subsequently the number of necessary simulations. The other solution consists of considering the species production as a unique parameter: the uncertainty corresponds to a factor, which is applied at each altitude, proportional to the error. In practice, it consists of computing the perturbed LR by multiplying the VER by the Monte-Carlo factor before integrating along the line of sight. If that factor corresponds to a normal law times the uncertainty for the VER, the resulting perturbed LR would follow a normal law from which we deduce the error by the usual means. This is equivalent to saying that the uncertainty comes only from a bias, which means that we maximize the estimation of the actual error. This technique allows us to speed up the computation without underestimating (and overestimating too much) the error, and therefore is used here for the LR uncertainty computation.

5.3. Application to Mars

[46] In the following, the VER and LR were computed, the latter with the hypothesis of a satellite at 200 km altitude scanning the limb with a tangent point altitude varying from 90 to 190 km. This is equivalent to observations with SPICAM (the satellite altitude is not important for the present simulation since the present emissions are negligible above 200 km).

5.3.1. Allowed Transitions

[47] The LR and VER values and corresponding uncertainties are presented in Figure 5 in the case of allowed transitions (or for transitions with a very short lifetime like the Cameron bands). In the left panel, the VER for CO_2^+(B) and CO($a^3\Pi$) are shown. The CO_2^+(B) state is only produced by electron and photon impact, so the VER is equal to the production presented in Figure 4. The CO($a^3\Pi$) state is also produced by dissociative recombination of CO_2^+. Even if it does not affect the altitude and intensity of the peak, one of the results of the recombination source is an increase of the production uncertainty below the peak, resulting in uncertainties larger than 100% at 110 km altitude.

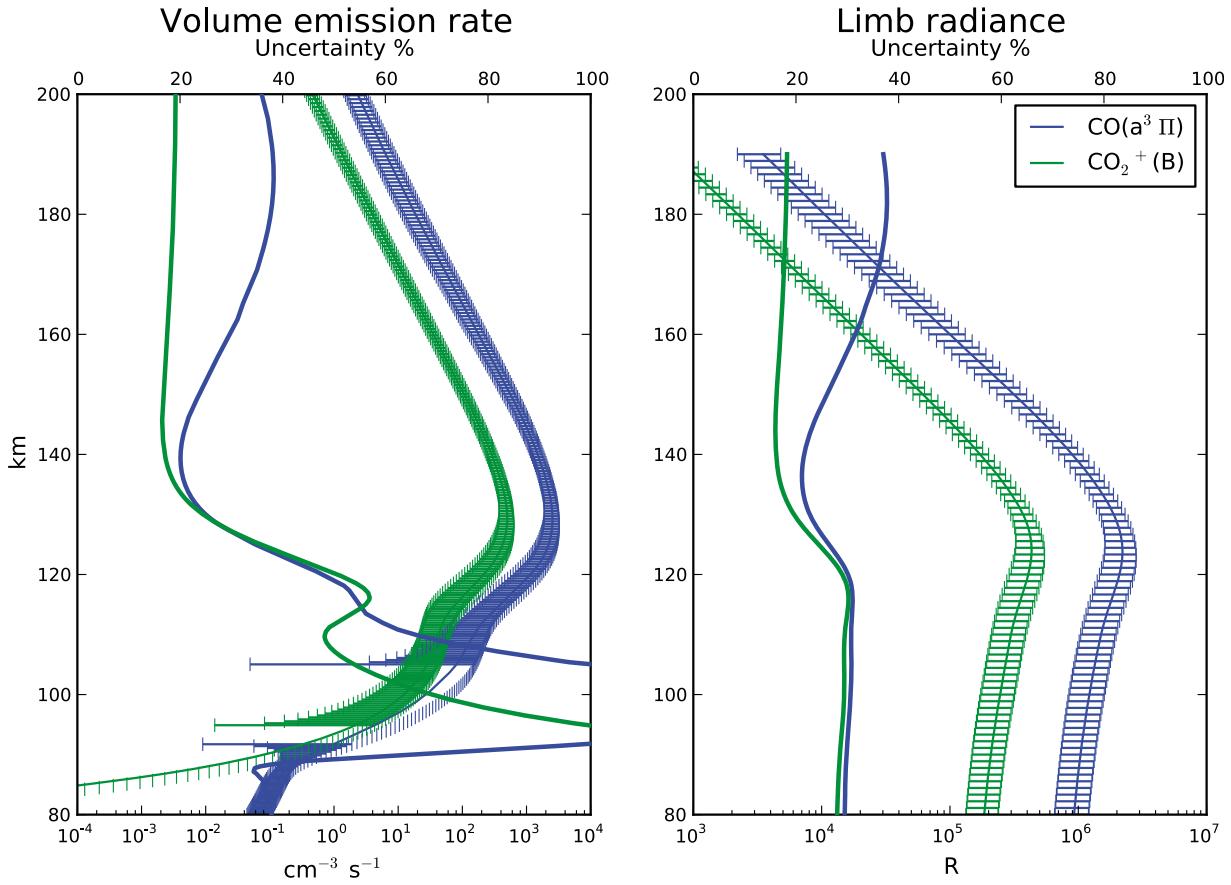

Figure 5. Uncertainties for the volume emission rate (VER) and limb radiance (LR) of the allowed transitions.

[48] In the right panel, the corresponding LR are computed. Above the ionization peak, the LR uncertainty is almost equal to the VER uncertainty: the main part of the observed radiance comes from the tangent point altitude (the contribution functions are peaked as in *Mertens et al.* [2009]) and therefore can be approximated by the VER at that altitude times a geometrical factor. Below the peak, a large part of the observed radiance comes from the altitude of the peak, and the uncertainties below this point are largely masked because of their negligible contribution to the total signal.

[49] In the frame of remote sensing applications, the objective is to retrieve the VER from the LR. Usually, an Abel inversion is used [*Solomon et al.*, 1984]. From the above considerations, it appears obvious that small observational uncertainties for the peak radiance implies large uncertainties for the inverted data below the peak. Therefore, the CO_2^+(B) transition, with a VER-LR uncertainty of 20% above the ionization peak, is an interesting target for retrieval purposes.

5.3.2. Forbidden Transitions

[50] For forbidden transitions, two parameters are to be considered: the chemical uncertainties (reaction rates, including the Einstein emission coefficients) and the production uncertainties. In Figure 6 the emission uncertainties due only to the chemistry are computed, and in Figure 7 all the sources are included.

[51] When compared with Figure 4, it appears that the VER of O(^{1}S) 557.7 nm is almost equal to the production of O(^{1}S) itself. This is due to a small quenching of O(^{1}S) by the neutral species. Consequently, a very small uncertainty is observed for the chemical reaction (Figure 6), caused almost entirely by the O_2^+ dissociative recombination uncertainty and mainly visible at 120 km, below the main O(^{1}S) production peak. For the 297.2 nm emission, the chemical uncertainty is more important, corresponding to the effect of the Einstein coefficient uncertainty. The consequence of that is the VER uncertainty in Figure 7: almost equal to the O(^{1}S) production uncertainty but with a little increase for O(^{1}S) 297.2 nm, which can be approximated by the square root of the sum of the squared production uncertainty and the squared chemical uncertainty.

[52] Concerning O(^{1}D), for which the total emission is computed in the figures, the situation is different: this state is very efficiently quenched and is mainly produced by the dissociative recombination of O_2^+ and the cascade from the O(^{1}S) state. This results in an emission uncertainty essentially decoupled from the electron and photon production uncertainty. It is therefore necessary to compute the whole uncertainty at once for this emission: it is not possible to compute the uncertainties independently and easily deduce the final uncertainty, in contrast with e.g. the solar and production uncertainties [*Gronoff et al.*, 2012]. The computation of the uncertainty for each state of the triplet is

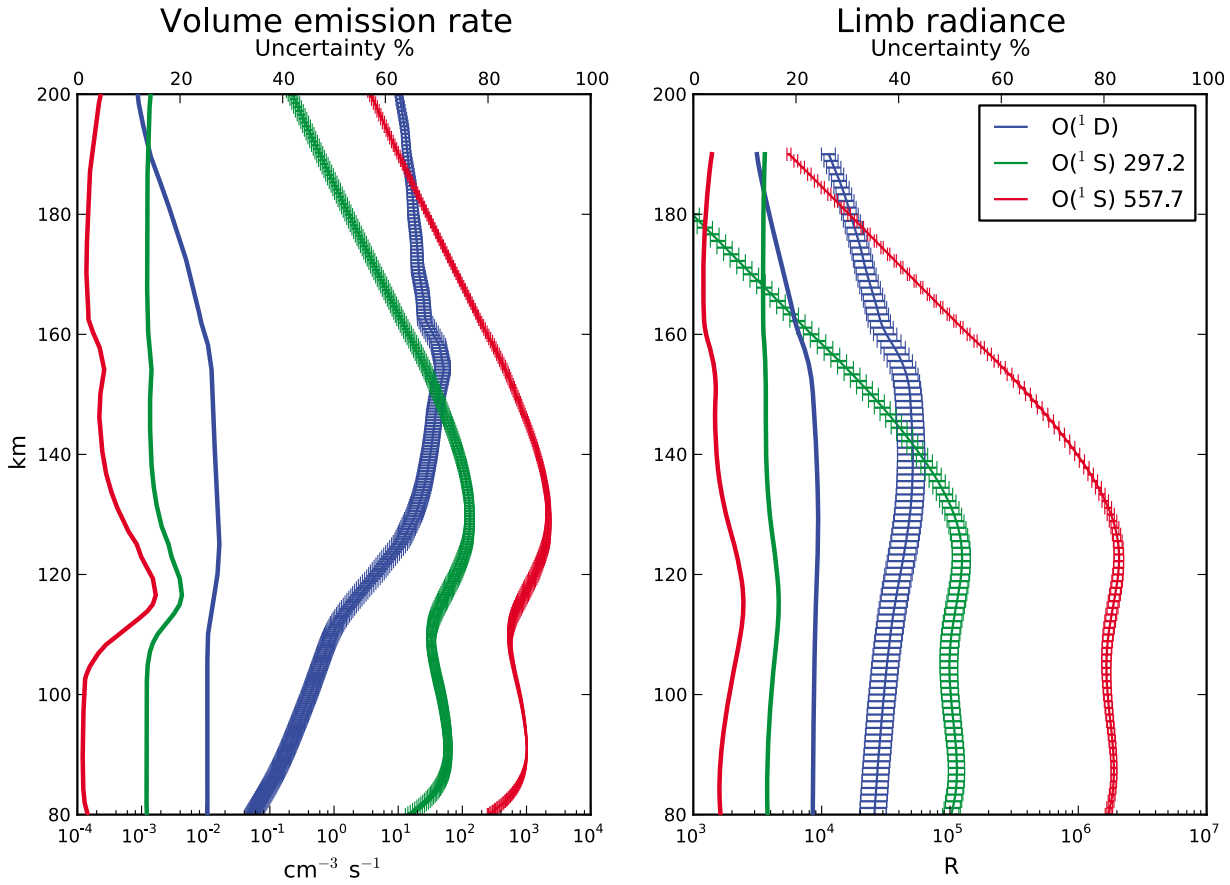

Figure 6. Uncertainties for the VER and LR of the forbidden transitions, when only the chemical reaction rates uncertainties are taken into account.

straightforward, even when considering the Einstein coefficient uncertainties.

[53] For the forbidden transitions, the passage from VER to LR is similar to that of the allowed transitions. The O(^{1}S) double peak provides in this respect valuable information below the main emission peak, and can usefully complement the successful retrieval performed with the CO_2^+(B) emissions. This will be developed in a future paper.

5.3.3. Influence of the Solar Flux Uncertainties

[54] When the uncertainties due to the solar flux are taken into account following the SEE uncertainty as computed in *Gronoff et al.* [2012] (Figure 8), the uncertainties are modified consistently with the modification in the species production uncertainty. The uncertainties for O(^{1}D) are unchanged because they are controlled by the chemistry. The LR uncertainties for O(^{1}S) is shifted to 30%. The main difference is the CO_2^+(B) uncertainty which become more important than the CO(a$^3\Pi$) one below 140 km with a limb radiance uncertainty of 40% below 120 km, and of the order of 30% above 130 km. The CO(a$^3\Pi$) LR uncertainty varies between 30% at 140 km to 35% above 160 km and below 120 km.

5.3.4. Comparison with SPICAM

[55] The *Aeroplanets* model results have been compared with SPICAM data [*Simon et al.*, 2009] to ensure the quality of the uncertainty and to verify that important biases (due, for example, to an unknown production mechanism) do not appear. The dataset for 21 January 2005 for Ls = 148 was chosen on the basis of minimal straylight. The model uses the corresponding SEE solar flux data [*Woods et al.*, 2005]. The first step of the comparison was to fit the CO_2 neutral atmosphere with the CO_2^+(B) emission. The fitted function was the sum of two exponentials [*Gronoff et al.*, 2010] which is sufficient for the present case. This fit gave a corrective factor for the gain of the SPICAM instrument, correction subsequently applied on the Cameron bands, CO_2^+(B) and O(^{1}S) 297.2 nm data (Figure 3). The fit was made between 120 km and 160 km, where more than 95% of the atmosphere is composed of CO_2. The influence of the other gases is negligible for the present study and their densities have not been fitted or corrected (the present team is preparing a paper discussing this technique, its uncertainties, and its application to the SPICAM data). The *Aeroplanets* model was then used to model the limb radiances and their uncertainties for these conditions, resulting in the modeled curves in Figure 3. Only uncertainties in production and chemical reaction rates were taken into account, not those in solar flux: the largest solar flux uncertainty is a calibration bias in intensity, and then the relative variation of the spectrum (the relative uncertainty in *Woods et al.* [2005]). The latter brings an uncertainty smaller than the cross section and chemical uncertainties and can therefore be neglected, while the former multiplies the production by a given factor. Since the calibration uncertainty bias is corrected in the fitting

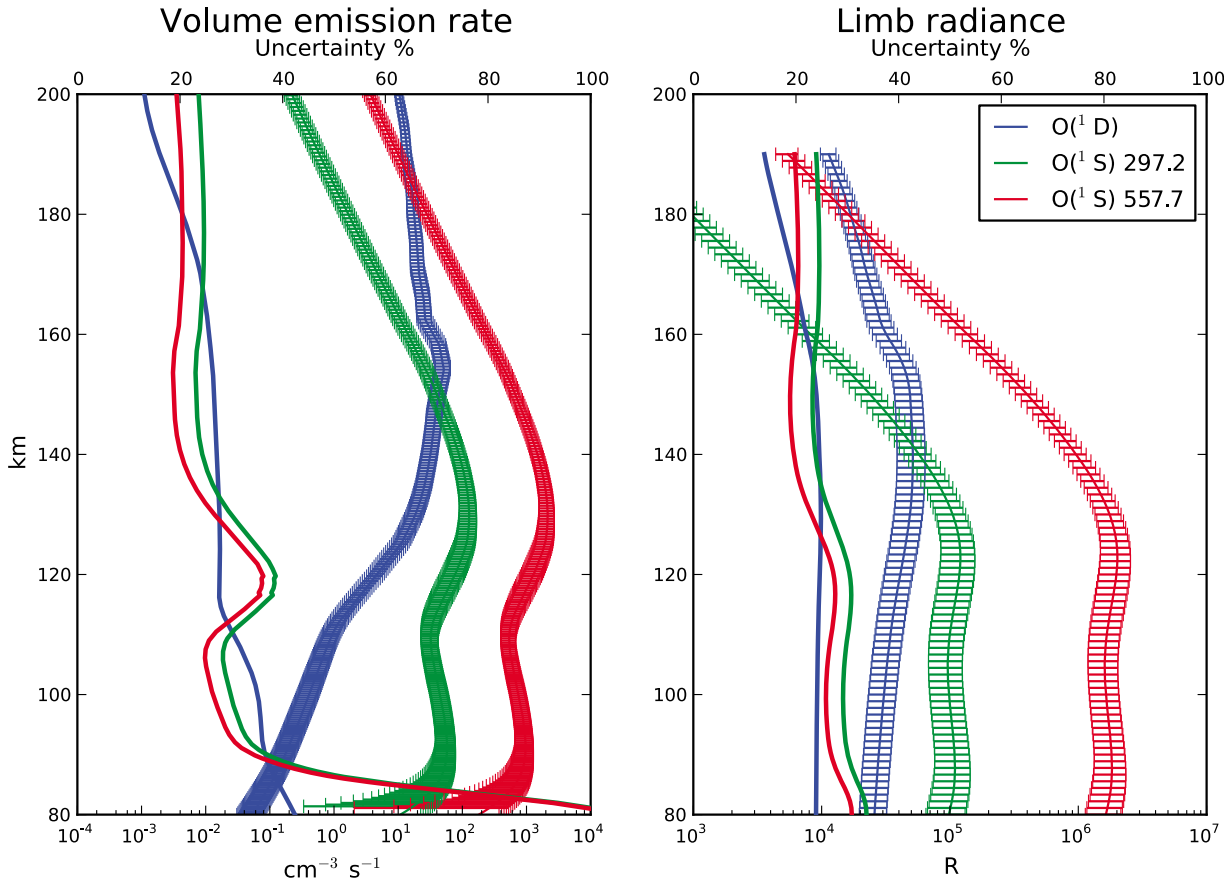

Figure 7. Uncertainties for the VER and LR of the forbidden transitions, when chemical reaction rates and species production uncertainties are taken into account.

process, the largest influence of the solar flux uncertainty is automatically corrected while all other solar uncertainty may be neglected.

[56] As demonstrated by the fit, the $CO_2^+(B)$ emission shows excellent agreement between the model and the data, the modeled curve being always within the error bars of the data.

[57] For the 297.2 emission, two LR curves were modeled following the discussion in section 4.5: one with the ratio 557.7/297.2 nm at 16 (lower radiance), the other with a ratio of 10. The data uncertainties are quite important, but the model and data error bars are always overlapping, for both emission ratios. This means that it is not currently possible with the SPICAM observations to discriminate between the theoretical approach (NIST) and that of *Slanger et al.* [2006b]; in fact, the recommended ratio of 10 for Earth by *Slanger et al.* [2006b] remains compatible with the observations at Mars. A possibility could be that the ratio of 10 along with a less efficient green line production could be the explanation for that emission. A better evaluation of the $O(^1S)$ yield from CO_2 photodissociation, as well as a more precise observation of the 297.2 line would be necessary for such a claim.

[58] For the Cameron bands, the data and the model error bars overlap everywhere except in the 160–170 km range. This is probably due to an underestimation of the error bars for the SPICAM observations: the uncertainty has been computed from the square root of the signal, but the Cameron bands being a set of emission, the uncertainty in the background has not been taken into account in the error bar evaluation. New data analysis are being performed to improve the estimation of these error bars. Close to the peak and below, model and observations are in good agreement. When using the original cross section for the electron impact on CO_2 (see section 3.2), the simulation results lie outside the SPICAM uncertainties below 120 km. This confirms *a posteriori* our previous evaluation of the correction for the *e*-CO_2 cross section and its estimation at a 25% uncertainty (see section 3.2).

6. Discussion

[59] The uncertainty analysis of the simulated lines of $O(^1S)$, $CO(a^3\Pi)$, and $CO_2^+(B)$ allows us to constrain the expectations on the Mars atmosphere retrieved parameters, which are beyond the scope of the present paper, and to define the best strategy for these retrievals. From a practical point of view, experimental parameters should also be taken into account for the selection of the best line or band for the retrieval. The intensity of the emission should therefore be taken into consideration, as well as lines overlapping and contamination of the spectrum by stray light. The Cameron

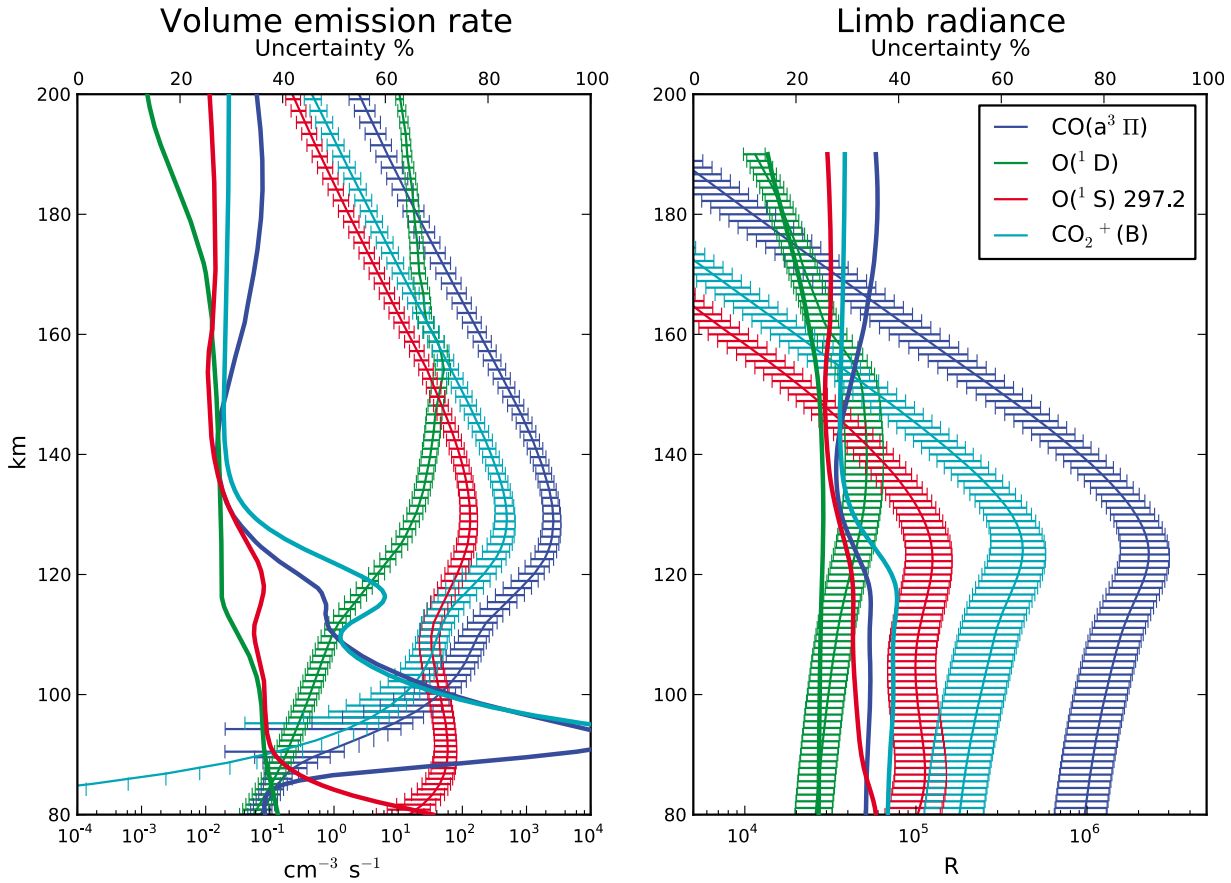

Figure 8. Uncertainties for the VER and LR of the considered transitions, when the solar flux, the chemical reaction rates and the species production uncertainties are taken into account.

bands are a good illustration of that problem: on paper, they have the intensity advantage over $CO_2^+(B)$ and a small emission uncertainty advantage just over the peak. Unfortunately, the Cameron bands are dispersed over a large set of wavelengths, which increases the uncertainties in the determination of the intensity from the spectrum. When the SPICAM data for these bands are considered, the presence of a Sapphire window (which cuts order overlapping on the spectrum) adds calibration uncertainties. Concerning the O(^{1}S) emission, the smaller uncertainty is balanced by a smaller intensity but also, in the SPICAM data, by more contamination, which increases the experimental uncertainties. It is possible to create dedicated experiments for the observation of the lines or bands in order to reduce the experimental uncertainties. The best example of that would be a limb instrument observing the 557.7 nm emission of O(^{1}S); it would have the advantage of the intensity (the 557.7 nm line is ten times stronger than the 297.2 nm line) as well as the advantage of a well-constrained uncertainty.

7. Conclusion

[60] Study of the uncertainties of the ionosphere-airglow models for the atmosphere of Mars allowed us to improve the interpretation of the SPICAM observations. From the computation of these error bars, we confirmed that CO_2 photodissociation is the main source of O(^{1}S) in the upper atmosphere of Mars. We showed that the cross-section for electron impact on CO_2 creating CO(a^{3}Π) should be divided by three in *Avakyan et al.* [1998] to agree with both observation and theory, validating the approaches of *Simon et al.* [2009] and *Jain and Bhardwaj* [2011b]. And, finally, we show that the modification of the 557.7 nm/297.2 nm O(^{1}S) emission ratio, observed at Earth, is compatible with the 297.2 emission computed and observed at Mars.

[61] Considering that the airglow models are used to retrieve the atmospheric parameters, the characterization of the model uncertainties puts a lower limit on the uncertainties for the retrieved parameters. The present work has shown that the emissions observed by SPICAM are now understood sufficiently to perform some remote sensing with a TIMED/SABER approach in the Martian upper atmosphere. However, the sensitivity of these emissions to the different parameters to be retrieved must be studied, along with the sensitivity of the instruments doing the observations for the remote sensing. To that extent, instrumentation using radiation-hard wide band gap technology will be more sensitive in the spectral range under consideration—near UV and visible—and particularly adapted for long duration missions (S. Aslam, personal communication, 2011). Finally, this work adds support to the development of embedded solar flux detector for planetary aeronomy missions, like the EUV instrument planned for the 2013 NASA MAVEN Mars Scout mission.

[62] **Acknowledgments.** The authors are indebted to Jean Lilensten (IPAG, France), Shahid Aslam (NASA GSFC, USA) and Arun Gopalan (SSAI/NASA, USA) for useful discussions. The authors wish to thank the anonymous referees for their numerous comments, suggestions, and corrections. The work of G. Gronoff was supported by an appointment to the NASA Postdoctoral Program at NASA Langley Research Center, administered by Oak Ridge Associated University through a contract with NASA and funded by the NASA Science Mission Directorate. The work of R. Lillis was funded by NASA Mars Fundamental Research Program grant NNX09AD43G and the NASA Mars Data Analysis Program grants NNX08AK94G and NNX11AI87G. C. Simon Wedlund received support from the Belgian BELSPO-PPS Science Policy through the Action 1 contracts MO/35/019 and MO/35/025.

[63] Robert Lysak thanks the reviewers for their assistance in evaluating this paper.

References

Ajello, J. M. (1971), Emission cross sections of CO_2 by electron impact in the interval 1260–4500 Å. II, *J. Chem. Phys.*, *55*(7), 3169–3177.

Atkinson, R., and K. H. Welge (1972), Temperature dependence of $O(^1S)$ deactivation by CO_2, O_2, N_2, and Ar, *J. Chem. Phys.*, *57*(9), 3689–3693.

Atkinson, R., D. L. Baulch, R. A. Cox, J. N. Crowley, R. F. Hampson, R. G. Hynes, M. E. Jenkin, M. J. Rossi, and J. Troe (2004), Evaluated kinetic and photochemical data for atmospheric chemistry: Volume I – Gas phase reactions of O_x, HO_x, NO_x and SO_x species, *Atmos. Chem. Phys.*, *4*, 1461–1738.

Avakyan, S. V., R. llin, V. Lavrov, and G. N. Ogurtsov (1998), *Collision Processes and Excitation of Ultraviolet Emission From Planetary Atmospheric Gases: A Handbook of Cross Sections*, Gordon and Breach, London.

Baluja, K. L., and C. J. Zeippen (1988), M1 and E2 transition probabilities for states within the $2p^4$ configuration of the O I isoelectronic sequence, *J. Phys. B*, *21*, 1455–1471.

Barth, C. A., and A. F. Hildebrandt (1961), The 5577 A airglow emission mechanism, *J. Geophys. Res.*, *66*(3), 985–986, doi:10.1029/JZ066i003p00985.

Barthélemy, M., C. Parkinson, J. Lilensten, and R. Prangé (2004), Modelling the Lyman β dayglow in the Jovian atmosphere, *Astron. Astrophys.*, *423*, 391–395.

Barthélemy, M., J. Y. Chaufray, J. Lilensten, C. Simon, C. Parkinson, and G. Gronoff (2010), Radiative transfer of the oxygen 130 nm triplet in atmospheres containing oxygen and carbon monoxyde, Abstract EPSC2010-633 presented at the 2010 European Planetary Science Congress, Rome, Italy, 19–24 Sept. [Available at http://meetings.copernicus.org/epsc2010.]

Berrington, K. A., and P. G. Burke (1981), Effective collision strengths for forbidden transitions in e-N and e-O scattering, *Planet. Space Sci.*, *29*, 377–381.

Bevington, P. R., and D. K. Robinson (2003), *Data Reduction and Error Analysis for the Physical Sciences*, 3rd ed., McGraw-Hill, Boston, Mass.

Blelly, P., C. Lathuillère, B. Emery, J. Lilensten, J. Fontanari, and D. Alcaydé (2005), An extended TRANSCAR model including ionospheric convection: simulation of EISCAT observations using inputs from AMIE, *Ann. Geophys.*, *23*, 419–431.

Bougher, S. W., S. Engel, D. P. Hinson, and J. M. Forbes (2001), Mars Global Surveyor Radio Science electron density profiles: Neutral atmosphere implications, *Geophys. Res. Lett.*, *28*, 3091–3094.

Bougher, S. W., S. Engel, D. P. Hinson, and J. R. Murphy (2004), MGS Radio Science electron density profiles: Interannual variability and implications for the Martian neutral atmosphere, *J. Geophys. Res.*, *109*, E03010, doi:10.1029/2003JE002154.

Cahoy, K. L., D. P. Hinson, and G. L. Tyler (2006), Radio science measurements of atmospheric refractivity with Mars Global Surveyor, *J. Geophys. Res.*, *111*, E05003, doi:10.1029/2005JE002634.

Cahoy, K. L., D. P. Hinson, and G. L. Tyler (2007), Characterization of a semidiurnal eastward-propagating tide at high northern latitudes with Mars Global Surveyor electron density profiles, *Geophys. Res. Lett.*, *34*, L15201, doi:10.1029/2007GL030449.

Capetanakis, F. P., F. Sondermann, S. Höser, and F. Stuhl (1993), Temperature dependence of the quenching of $O(^1S)$ by simple inorganic molecules, *J. Chem. Phys.*, *98*(10), 7883–7887.

Chaufray, J. Y., F. Leblanc, E. Quémerais, and J. L. Bertaux (2009), Martian oxygen density at the exobase deduced from O I 130.4-nm observations by Spectroscopy for the Investigation of the Characteristics of the Atmosphere of Mars on Mars Express, *J. Geophys. Res.*, *114*, E02006, doi:10.1029/2008JE003130.

Conway, R. R. (1981), Spectroscopy of the Cameron bands in the Mars airglow, *J. Geophys. Res.*, *86*(A6), 4767–4775, doi:10.1029/JA086iA06p04767.

Cox, C., J.-C. Gérard, B. Hubert, J.-L. Bertaux, and S. W. Bougher (2010), Mars ultraviolet dayglow variability: SPICAM observations and comparison with airglow model, *J. Geophys. Res.*, *115*, E04010, doi:10.1029/2009JE003504.

Culot, F., C. Lathuillère, and J. Lilensten (2005), Influence of geomagnetic activity on the O I 630.0 and 557.7 nm dayglow, *J. Geophys. Res.*, *110*, A01304, doi:10.1029/2004JA010667.

Doering, J. P. (1992), Absolute differential and integral electron excitation cross sections for atomic oxygen, 9. Improved cross section for the $^3P \rightarrow {}^1D$ transition from 4.0 to 30 eV, *J. Geophys. Res.*, *97*(A12), 19,531–19,534, doi:10.1029/92JA02007.

Dreyer, J. W., D. Perner, and C. R. Roy (1974), Rate constants for the quenching of $N_2(A^3\Sigma_u^+,\ \nu = 0–8)$ by CO, CO_2, NH_3, NO, and O_2, *J. Chem. Phys.*, *61*(8), 3164–3169.

Dudok de Wit, T., J. Lilensten, J. Aboudarham, P. Amblard, and M. Kretzschmar (2005), Retrieving the solar EUV spectrum from a reduced set of spectral lines, *Ann. Geophys.*, *23*, 3055–3069.

Dudok de Wit, T., M. Kretzschmar, J. Aboudarham, P. Amblard, F. Auchère, and J. Lilensten (2008), Which solar EUV indices are best for reconstructing the solar EUV irradiance?, *Adv. Space Res.*, *42*, 903–911.

Dunlea, E. J., and A. R. Ravishankara (2004), Kinetic studies of the reactions of $O(^1D)$ with several atmospheric molecules, *Phys. Chem. Chem. Phys.*, *6*(9), 2152–2161, doi:10.1039/b400247d.

Durrance, S. T. (1981), The carbon monoxide fourth positive bands in the Venus dayglow, 1. Synthetic spectra, *J. Geophys. Res.*, *86*(A11), 9115–9124, doi:10.1029/JA086iA11p09115.

Erdman, P. W., and E. C. Zipf (1983), Electron-impact excitation of the Cameron system ($a^3\Pi$ yields $X^1\Sigma$) transition of CO, *Planet. Space Sci.*, *31*, 317–321.

Feldman, P. D., C. B. Opal, R. R. Meier, and K. R. Nicolas (1976), Far ultraviolet excitation processes in comets, in *The Study of Comets, Part 2*, edited by B. Donn et al., pp. 773–796, NASA Sci. and Tech. Inf. Off., Washington, D. C.

Feldman, P. D., et al. (2010), Rosetta-Alice observations of exospheric hydrogen and oxygen on Mars, Poster P53E-1569 presented at 2010 Fall Meeting, AGU, San Francisco, Calif., 13–17 Dec.

Feldman, P. D., et al. (2011), Rosetta-Alice observations of exospheric hydrogen and oxygen on Mars, *Icarus*, *214*(2), 394–399, doi:10.1016/j.icarus.2011.06.013.

Forbes, J. M., F. G. Lemoine, S. L. Bruinsma, M. D. Smith, and X. Zhang (2008), Solar flux variability of Mars' exosphere densities and temperatures, *Geophys. Res. Lett.*, *35*, L01201, doi:10.1029/2007GL031904.

Forget, F., F. Montmessin, J. Bertaux, F. González-Galindo, S. Lebonnois, E. Quémerais, A. Reberac, E. Dimarellis, and M. A. López-Valverde (2009), Density and temperatures of the upper Martian atmosphere measured by stellar occultations with Mars Express SPICAM, *J. Geophys. Res.*, *114*, E01004, doi:10.1029/2008JE003086.

Fox, J. L. (2009), Morphology of the dayside ionosphere of Mars: Implications for ion outflows, *J. Geophys. Res.*, *114*, E12005, doi:10.1029/2009JE003432.

Fox, J. L., and S. W. Bougher (1991), Structure, luminosity, and dynamics of the Venus thermosphere, *Space Sci. Rev.*, *55*, 357–489.

Fox, J. L., and K. Y. Sung (2001), Solar activity variations of the Venus thermosphere/ionosphere, *J. Geophys. Res.*, *106*(A10), 21,305–21,335, doi:10.1029/2001JA000069.

Frederick, J. E., D. W. Rusch, G. A. Victor, W. E. Sharp, P. B. Hays, and H. C. Brinton (1976), The O I λ5577 Å airglow: Observations and excitation mechanisms, *J. Geophys. Res.*, *81*(22), 3923–3930, doi:10.1029/JA081i022p03923.

García Muñoz, A., F. P. Mills, T. G. Slanger, G. Piccioni, and P. Drossart (2009), Visible and near-infrared nightglow of molecular oxygen in the atmosphere of Venus, *J. Geophys. Res.*, *114*, E12002, doi:10.1029/2009JE003447.

Gattinger, R. L., N. D. Lloyd, A. E. Bourassa, D. A. Degenstein, I. C. McDade, and E. J. Llewellyn (2009), Observation of the 557.7 nm to 297.2 nm brightness ratio in the auroral spectrum with OSIRIS on Odin, *Can. J. Phys.*, *87*(10), 1133–1137, doi:10.1139/P09-102.

Gilijamse, J. J., S. Hoekstra, S. A. Meek, M. Metsälä, S. Y. T. van de Meerakker, G. Meijer, and G. C. Groenenboom (2007), The radiative lifetime of metastable CO ($a^3\Pi$, $\nu = 0$), *J. Chem. Phys.*, *127*(22), 221102-1–221102-4.

Gronoff, G., J. Lilensten, C. Simon, O. Witasse, R. Thissen, O. Dutuit, and C. Alcaraz (2007), Modelling dications in the diurnal ionosphere of Venus, *Astron. Astrophys.*, *465*(2), 641–645, doi:10.1051/0004-6361:20065991.

Gronoff, G., J. Lilensten, C. Simon, M. Barthélemy, F. Leblanc, and O. Dutuit (2008), Modelling the Venusian airglow, *Astron. Astrophys.*, *482*(3), 1015–1029, doi:10.1051/0004-6361:20077503.

Gronoff, G., C. Simon, C. J. Mertens, and J. Lilensten (2010), Advances in remote sensing of the Martian upper atmosphere, Poster SA11A–1560 presented at 2010 Fall Meeting, AGU, San Francisco, Calif. 13–17 Dec.

Gronoff, G., C. Simon Wedlund, C. J. Mertens, and R. J. Lillis (2012), Computing uncertainties in ionosphere-airglow models: I. Electron flux and species production uncertainties for Mars, *J. Geophys. Res.*, *117*, A04306, doi:10.1029/2011JA016930.

Herron, J. T. (1999), Evaluated chemical kinetics data for reactions of $N(^2D)$ $N(^2P)$, and $N_2(A^3\Sigma_u^+)$ in the gas phase, *J. Phys. Chem. Ref. Data*, *28*(5), 1453–1484, doi:10.1063/1.556043.

Hill, S. M., S. C. Solomon, D. D. Cleary, and A. L. Broadfoot (2000), Temperature dependence of the reaction $N_2(A^3\Sigma_u^+)$ + O in the terrestrial thermosphere, *J. Geophys. Res.*, *105*(A5), 10,615–10,629, doi:10.1029/1999JA000395.

Huestis, D. L., T. G. Slanger, B. D. Sharpee, and J. L. Fox (2010), Chemical origins of the Mars ultraviolet dayglow, *Faraday Discuss.*, *147*, 307–322, doi:10.1039/c003456h.

Huntress, W. T., Jr., and V. G. Anicich (1976), On the reaction of N^+ ions with O_2, *Geophys. Res. Lett.*, *3*(6), 317–318, doi:10.1029/GL003i006p00317.

Jain, S. K., and A. Bhardwaj (2011a), Model calculation of N_2 Vegard-Kaplan band emissions in Martian dayglow, *J. Geophys. Res.*, *116*, E07005, doi:10.1029/2010JE003778.

Jain, S. K., and A. Bhardwaj (2011b), Impact of solar EUV flux on CO cameron band and CO_2^+ UV doublet emissions in the dayglow of Mars, *Planet. Space Sci.*, *63–64*, 110–122, doi:10.1016/j.pss.2011.08.010.

Johnson, C. E. (1972), Lifetime of $CO(a^3\Pi)$ following electron impact dissociation of CO_2, *J. Chem. Phys.*, *57*(1), 576–577, doi:10.1063/1.1678007.

Kalogerakis, K. S., T. G. Slanger, E. A. Kendall, T. R. Pedersen, M. J. Kosch, B. Gustavsson, and M. T. Rietveld (2009), Remote oxygen sensing by ionospheric excitation (ROSIE), *Ann. Geophys.*, *27*, 2183–2189.

Kassal, T. (1975), Resonant fluorescent scattering of solar radiation by the fourth positive band system of CO, *Appl. Opt.*, *14*(7), 1513–1515, doi:10.1364/AO.14.001513.

Kassal, T. T. (1976), Scattering of solar Lyman Alpha by the (14, 0) band of the fourth positive system of CO, *J. Geophys. Res.*, *81*(7), 1411–1412, doi:197610.1029/JA081i007p01411.

Kella, D., L. Vejby-Christensen, P. J. Johnson, H. B. Pedersen, and L. H. Andersen (1997), The source of green light emission determined from a Heavy-Ion storage ring experiment, *Science*, *276*(5318), 1530–1533, doi:10.1126/science.276.5318.1530.

Kopp, J. P., J. E. Frederick, D. W. Rusch, and G. A. Victor (1977), Morning and evening behavior of the F region green line emission: Evidence concerning the sources of $O(^1S)$, *J. Geophys. Res.*, *82*(29), 4715–4719, doi:10.1029/JA082i029p04715.

Krauss, M., and D. Neumann (1975), On the interaction of $O(^1S)$ with $O(^3P)$, *Chem. Phys. Lett.*, *36*, 372–374.

Langford, A. O., V. M. Bierbaum, and S. R. Leone (1986), Branching ratios for electronically excited oxygen atoms formed in the reaction of N^+ with O_2 at 300 K, *J. Chem. Phys.*, *84*(4), 2158–2166.

LeCompte, M. A., L. J. Paxton, and A. I. F. Stewart (1989), Analysis and interpretation of observations of airglow at 297 nm in the Venus thermosphere, *J. Geophys. Res.*, *94*(A1), 208–216, doi:198910.1029/JA094iA01p00208.

Link, R., and P. K. Swaminathan (1992), $N(^2D) + O_2$: A source of thermospheric 6300-A emission?, *Planet. Space. Sci.*, *40*, 699–705.

López-Puertas, M., and F. W. Taylor (2001), *Non-LTE Radiative Transfer in the Atmosphere, Ser. on Atmos. Ocean. and Planet. Phys.*, vol. 3, 504 pp., World Sci., Republic of Singapore.

Mantas, G. P. (1994), Large 6300-Å airglow intensity enhancements observed in ionosphere heating experiments are excited by thermal electrons, *J. Geophys. Res.*, *99*(A5), 8993–9002, doi:10.1029/94JA00347.

McDade, I. C., D. P. Murtagh, R. G. H. Greer, P. H. G. Dickinson, G. Witt, J. Stegman, E. J. Llewellyn, L. Thomas, and D. B. Jenkins (1986), ETON 2: Quenching parameters for the proposed precursors of $O2(b^1\Sigma_g^+)$ and $O(^1S)$ in the terrestrial nightglow, *Planet. Space Sci.*, *34*(9), 789–800, doi:16/0032-0633(86)90075-9.

Mehr, F. J., and M. A. Biondi (1969), Electron temperature dependence of recombination of O_2^+ and N_2^+ ions with electrons, *Phys. Rev.*, *181*, 264–271.

Meier, R. R. (1991), Ultraviolet spectroscopy and remote sensing of the upper atmosphere, *Space Sci. Rev.*, *58*, 1–185, doi:10.1007/BF01206000.

Mertens, C. J., et al. (2009), Kinetic temperature and carbon dioxide from broadband infrared limb emission measurements taken from the TIMED/SABER instrument, *Adv. Space Res.*, *43*(1), 15–27, doi10.1016/j.asr.2008.04.017.

Murtagh, D., G. Witt, J. Stegman, I. McDade, E. Llewellyn, F. Harris, and R. Greer (1990), An assessment of proposed $O(^1S)$ and $O_2(b^1\Sigma_g^+)$ nightglow excitation parameters, *Planet. Space Sci.*, *38*(1), 43–53, doi:16/0032-0633(90)90004-A.

Parisot, J.-P. (1986), Excitation of Herzberg I and II bands in the atmospheres of Earth and Venus, *Ann. Geophys.*, *4*, 481–486.

Parkinson, C. (2002), Photochemistry and radiative transfer studies in the atmospheres of Jupiter and Saturn, PhD thesis, Dep. of Earth and Space Sci., York University, North York, Ontario, Canada.

Pätzold, M., et al. (2007), The structure of Venus' middle atmosphere and ionosphere, *Nature*, *450*, 657–660.

Petrignani, A., W. J. van der Zande, P. C. Cosby, F. Hellberg, R. D. Thomas, and M. Larsson (2004), Vibrationally resolved rate coefficients and branching fractions in the dissociative recombination of O_2^+, *J. Chem. Phys.*, *122*(1), 014302, doi:10.1063/1.1825991.

Peverall, R., et al. (2000), The ionospheric oxygen Green airglow: Electron temperature dependence and aeronomical implications, *Geophys. Res. Lett.*, *27*(4), 481–484, doi:10.1029/1999GL010711.

Peverall, R., et al. (2001), Dissociative recombination and excitation of O_2^+: Cross sections, product yields and implications for studies of ionospheric airglows, *J. Chem. Phys.*, *114*(15), 6679–6689.

Piper, L. G. (1993), Reevaluation of the transition-moment function and Einstein coefficients for the $N_2(A^3\Sigma_u^+ - X^1\Sigma_g^+)$ transition, *J. Chem. Phys.*, *99*(5), 3174–3181.

Ralchenko, Y., A. Kramida, J. Reader, and NIST ASD Team (2010), National Institute of Standards and Technology Atomic Spectra Database (Version 4.0.1), http://physics.nist.gov/asd, Dep. of Commer., Washington, D. C.

Rawlins, W. T., M. E. Fraser, and S. M. Miller (1989), Rovibrational excitation of nitric oxide in the reaction of oxygen with metastable atomic nitrogen, *J. Phys. Chem.*, *93*(3), 1097–1107, doi:10.1021/j100340a016.

Rosén, S., et al. (1998), Absolute cross sections and final-state distributions for dissociative recombination and excitation of $CO^+(\nu = 0)$ using an ion storage ring, *Phys. Rev. A*, *57*, 4462–4471, doi:10.1103/PhysRevA.57.4462.

Schofield, K. (1978), Rate constants for the gaseous interactions of $O(2^1D_2)$ and $O(2^1S_0)$: A critical evaluation, *J. Photochem.*, *9*, 55–68.

Shematovich, V. I., D. V. Bisikalo, J.-C. Gérard, C. Cox, S. W. Bougher, and F. Leblanc (2008), Monte Carlo model of electron transport for the calculation of Mars dayglow emissions, *J. Geophys. Res.*, *113*, E02011, doi:10.1029/2007JE002938.

Simon, C., O. Witasse, F. Leblanc, G. Gronoff, and J. Bertaux (2009), Dayglow on Mars: Kinetic modelling with SPICAM UV limb data, *Planet. Space Sci.*, *57*, 1008–1021.

Simon Wedlund, C., G. Gronoff, and S. Bougher (2011), Exospheric temperatures at Mars measured by SPICAM: Seasonal trends, paper presented at the 2011 European Planetary Science Congress-Division for Planetary Science Joint Meeting in Nantes, France, 2–7 Oct.

Skrzypkowski, M., T. Gougousi, R. Johnsen, and M. F. Golde (1998), Measurement of the absolute yield of $CO(a^3\Pi)+O$ products in the dissociative recombination of CO_2^+ ions with electrons, *J. Chem. Phys.*, *108*(20), 8400–8407.

Slanger, T. G., and G. Black (1981), Quenching of $O(^1S)$ by $O_2(a^1\Delta_g)$, *Geophys. Res. Lett.*, *8*(5), 535–538, doi:10.1029/GL008i005p00535.

Slanger, T. G., P. C. Cosby, D. L. Huestis, and T. A. Bida (2001), Discovery of the atomic oxygen green line in the Venus night airglow, *Science*, *291*(5503), 463–465, doi:10.1126/science.291.5503.463.

Slanger, T., D. Huestis, P. Cosby, N. Chanover, and T. Bida (2006a), The Venus nightglow: Ground-based observations and chemical mechanisms, *Icarus*, *182*(1), 1–9, doi:10.1016/j.icarus.2005.12.007.

Slanger, T. G., P. C. Cosby, B. D. Sharpee, K. R. Minschwaner, and D. E. Siskind (2006b), $O(^1S \rightarrow {}^1D, {}^3P)$ branching ratio as measured in the terrestrial nightglow, *J. Geophys. Res.*, *111*, A12318, doi:10.1029/2006JA011972.

Snively, J. B., V. P. Pasko, and M. J. Taylor (2010), OH and OI airglow layer modulation by ducted short-period gravity waves: Effects of trapping altitude, *J. Geophys. Res.*, *115*, A11311, doi:10.1029/2009JA015236.

Solomon, S. C., P. B. Hays, and V. J. Abreu (1984), Tomographic inversion of satellite photometry, *Appl. Opt.*, *23*, 3409–3414.

Valeille, A., M. R. Combi, V. Tenishev, S. W. Bougher, and A. F. Nagy (2010), A study of suprathermal oxygen atoms in Mars upper thermosphere and exosphere over the range of limiting conditions, *Icarus*, *206*, 18–27.

Wells, W. C., W. L. Borst, and E. C. Zipf (1972), Production of $CO(a^3\Pi)$ and other metastable fragments by electron impact dissociation of CO_2, *J. Geophys. Res.*, *77*(1), 69–75, doi:10.1029/JA077i001p00069.

Witasse, O., J. Lilensten, C. Lathuillère, and P. L. Blelly (1999), Modeling the OI 630.0 and 557.7 nm thermospheric dayglow during EISCAT-WINDII coordinated measurements, *J. Geophys. Res.*, *104*(A11), 24,639–24,656, doi:10.1029/1999JA900260.

Withers, P. (2009), A review of observed variability in the dayside ionosphere of Mars, *Adv. Space Res.*, *44*(3), 277–307, doi:16/j.asr.2009.04.027.

Withers, P., S. Bougher, and G. Keating (2003), The effects of topographically-controlled thermal tides in the Martian upper atmosphere as seen by the MGS accelerometer, *Icarus*, *164*, 14–32, doi:16/S0019-1035(03)00135-0.

Woods, T. N., F. G. Eparvier, S. M. Bailey, P. C. Chamberlin, J. Lean, G. J. Rottman, S. C. Solomon, W. K. Tobiska, and D. L. Woodraska (2005), Solar EUV experiment (SEE): Mission overview and first results, *J. Geophys. Res.*, *110*, A01312, doi:10.1029/2004JA010765.

Zou, H., R. J. Lillis, J. S. Wang, and E. Nielsen (2011), Determination of seasonal variations in the Martian neutral atmosphere from observations of ionospheric peak height, *J. Geophys. Res.*, *116*, E09004, doi:10.1029/2011JE003833.